Indazolone-Based Molecular Glue Degraders as a Tunable Platform for Reprogramming Cereblon Substrate Specificity

Hui-Jun Nie[1 ‡], Jiamin Wang[2 ‡], Hao Xu[1, 5 ‡], Yin-Jue Zhou[1, 5], Guang-Liang Yin[1], Xiaomim Xu[3], Gaoya Xu[2], Beijing Chen[3], Xian Li[3], Xiaobei Hu[2, 3], Yubo Zhou[3], Jia Li[2, 3] * Xiao-Hua Chen[1, 4] *

[1] State Key Laboratory of Drug Research, Shanghai Institute of Materia Medica, Chinese Academy of Sciences, Shanghai, 201203, China.

[2] State Key Laboratory of Chemical Biology, Shanghai Institute of Materia Medica, Chinese Academy of Sciences, Shanghai, 201203, China.

[3] Zhongshan Institute for Drug Discovery, Shanghai Institute of Materia Medica, Chinese Academy of Sciences, Zhongshan 528400, China

[4] School of Pharmaceutical Science and Technology, Hangzhou Institute for Advanced Study, University of Chinese Academy of Sciences, Hangzhou, 310024, China.

[5] University of Chinese Academy of Sciences, Beijing, 100049, China.

‡ These authors contributed equally to this work.

***Corresponding Author(s):** Xiao-Hua Chen: xhchen@simm.ac.cn; Jia Li, jli@simm.ac.cn

Abstract

Molecular glue degraders (MGDs) represent a transformative modality in drug discovery. Notably, the cereblon (CRBN)-MGD axis offers a broad opportunity for therapeutic intervention, serving as a strategic gateway to systematically target the historically undruggable proteome. However, the limited chemical diversity of CRBN-mediated MGDs has critically impeded the full exploration of the degradable proteome. Here, we introduce an innovative indazolone-based platform that transcends the canonical isoindolinone-glutarimide scaffolds, thereby significantly expanding the chemical space for CRBN modulation. Guided by mechanistic insights into CRBN-MGD complex conformational plasticity, our rational design yielded novel indazolone architectures demonstrating potent CRBN binding and unprecedented substrate programmability. This platform enabled fine-tuned control over neo-substrate recognition, leading to diverse degradation profiles from multi-target to exquisitely selective for critical proteins like IKZF1/3, ZFP91, LIMD1, CK1α, and IKZF2. This work not only converts previously undruggable proteins into tractable therapeutic targets but also establishes novel strategies for challenging diseases, including hematological malignancies and solid tumors. Collectively, the indazolone-based architectures' remarkable tunability and favorable pharmacokinetic properties establish them as a powerful blueprint for next-generation MGD development, enabling systematic exploration of the vast CRBN-accessible target space. Furthermore, as superior CRBN ligands, they offer invaluable potential for both MGD and diverse PROTAC discovery to systematically address intractable diseases.

Keywords

Molecular glue degrader; CRBN ligand; Indazolone-based platform; Neo-substrate reprogramming; Targeted protein degradation;

Introduction

Targeted protein degradation (TPD) has emerged as a revolutionary paradigm in drug discovery, offering a transformative modality to eliminate previously undruggable proteins beyond the reach of conventional inhibition.[1-5] Unlike occupancy-based inhibitors, TPD harnesses the cell's endogenous proteostasis machinery to selectively degrade disease-associated proteins, thereby providing innovative therapeutic strategies for challenging targets pivotal in complex diseases.[1] Within the TPD realm, molecular glue degraders (MGDs) have garnered exceptional interest, primarily due to their distinct pharmacological advantages over heterobifunctional proteolysis-targeting chimeras (PROTACs), including lower molecular weight and superior drug-likeness.[1-4] Mechanistically, MGDs operate by orchestrating a topographical remodeling of E3 ligase surfaces, inducing neomorphic protein-protein interaction (PPI) interfaces that enable the recruitment of non-native substrates (neo-substrates).[6-10] Specifically, neo-substrate recognition is exquisitely sensitive to molecular geometry; even subtle structural perturbations to an MGD structure can profoundly reprogram the E3 ligase's substrate preference (Figure 1a).[8-10] Consequently, this unique capacity to redirect E3 specificity holds profound implications for drug discovery, ultimately offering transformative potential for systematically expanding the druggable proteome.[10-17]

The clinical validation of this reprogramming principle is exemplified by the immunomodulatory imide drugs (IMiDs)—including thalidomide, lenalidomide (LENA), and pomalidomide.[10, 18-20] These landmark therapeutics fundamentally demonstrated that small molecules can redirect the E3 ligase cereblon (CRBN) to eliminate critical oncogenic drivers, such as IKZF1/3[21-24] and CK1α[25-29] , thereby establishing CRBN as the preeminent hotspot for degrader discovery.[10-12, 20, 30] More importantly, this clinical success has not only marked a new era for targeting previously intractable proteins but has also catalyzed an intensive pursuit of CRBN next-generation MGDs targeting an expanding array of disease-associated proteins, including GSPT1,[31-34] IKZF2,[27, 35-38] WIZ, [39, 40] Wee1,[41] VAV1,[42] and NEK7.[43,44] Furthermore, beyond these established successes, recent systematic mining of the CRBN-accessible substrate space has unveiled an extraordinary, yet largely unexplored, proteomic breadth (Figure 1b).[11, 12, 16, 17] Genomic and structural profiling suggests that the human proteome harbors a vast repertoire of over 1,600 potential neo-substrates—spanning numerous essential transcription factors and kinases—that are theoretically susceptible to CRBN-mediated recruitment.[12] These targets can be engaged through a spectrum of recognition mechanisms, ranging from the recognition of cryptic structural motifs, such as helical G-loops, to the recruitment of substrates via non-canonical degrons. Therefore, the CRBN-MGD axis represents an extensive resource for therapeutic intervention, serving as a strategic gateway to systematically access the vast, historically undruggable proteome. [10-12, 16, 17, 20, 45]

However, despite this expansive theoretical degradome, a significant gap persists between the vast landscape of CRBN-accessible targets and the current chemical repertoire.[10-12] To date, the development of clinical and emerging CRBN-based MGDs has remained predominantly dependent upon the canonical isoindolinone glutarimide scaffold.[10, 46, 47] Given the stringent structural requirements for neo-substrate recognition and specificity, this over-reliance on isoindolinone glutarimide architecture may inadvertently restrict the degradable landscape to a narrow subset of the proteome,[11, 48] leaving vast regions of the target space unreachable.[15] Furthermore, while alternative CRBN-binding ligands, such as phenyl,[49] benzamide,[50] and anilino glutarimides,[51] as well as other aryl glutarimide derivatives,[26, 52, 53] have been successfully employed in heterobifunctional PROTAC development, their potential to function as monovalent MGD scaffolds for reprogramming substrate specificity remains largely underexplored.[54, 55] Consequently, the development of novel CRBN-engaging scaffolds beyond the traditional isoindolinone glutarimide paradigm represents a strategic necessity for the discovery of next-generation MGDs.[15, 46, 47, 50, 51] Such unprecedented architecture-driven exploration is poised to facilitate the discovery of novel MGDs, offering a profound opportunity to systematically expand the boundaries of the druggable proteome.[10, 56]

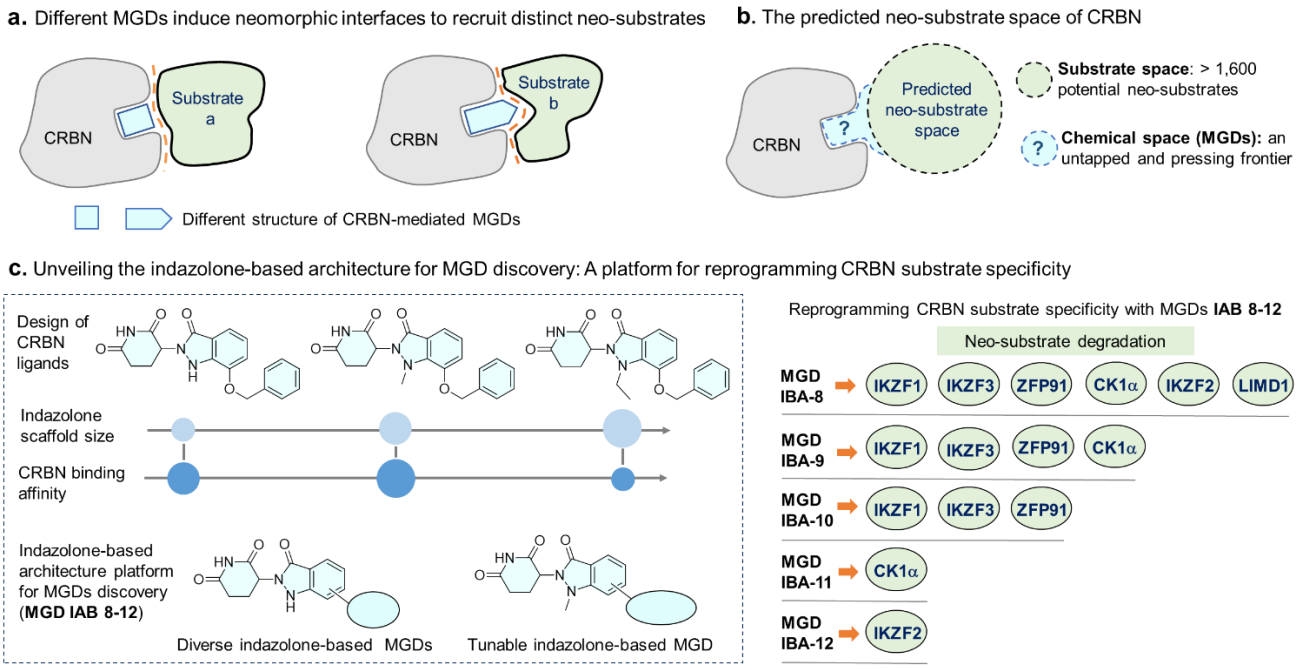

Figure 1. Mechanisms of CRBN neo-substrate recruitment and design of an indazolone-based MGD platform for reprogramming substrate specificity. a) MGD-induced neomorphic interfaces enabling selective substrate recruitment, and the predicted CRBN-accessible degradome. **b**) The predicted neo-substrate space of CRBN. **c**) Design of indazolone-based architectures as novel CRBN binders, and the development of structurally diverse MGDs to reprogram CRBN substrate specificity, thereby expanding the MGD-accessible degradome.

Herein, we introduce an innovative indazolone-based discovery platform that effectively expands the chemical space for CRBN-mediated MGDs (Figure 1c), successfully transcending the

architectural constraints of canonical isoindolinone-glutarimide scaffolds. Guided by mechanistic insights into the conformational plasticity of the CRBN-MGD complex, we rationally designed a diverse array of novel indazolone architectures. This platform demonstrates unprecedented programmability over E3 ligase substrate specificity. By leveraging the intrinsic tunability of the indazolone architecture, we achieved fine-tuned control over neosubstrate recognition, yielding a versatile spectrum of degradation profiles—ranging from potent multi-target degraders to exquisitely selective agents against critical oncogenic drivers, including IKZF1/3, ZFP91, LIMD1, CK1α, and IKZF2. Furthermore, our findings validate that this distinct chemotype not only maintains highly effective CRBN binding but also exhibits favorable pharmacokinetic properties, making it highly suitable for preclinical translation. By effectively decoupling MGD discovery from traditional structural limitations, this work provides a robust blueprint for converting historically undruggable proteins into tractable therapeutic targets, thereby establishing novel intervention strategies for challenging hematological malignancies and solid tumors. Collectively, as versatile and highly efficient CRBN ligands, this indazolone platform harbors immense potential to catalyze the development of next-generation MGDs and structurally diverse PROTACs, offering a powerful strategic gateway to systematically explore the vast CRBN-accessible target space and address intractable human diseases.

Results and discussion

Shifted Conformation-Inspired Design of Indazolone-Based Architectures as CRBN Binders

Structural insights from the recently reported CRBN-LENA-CK1α complex reveal a fascinating conformational adaptation within the CRBN E3 ligase (Figure 2a). Upon recruitment of the neo-substrate CK1α, LENA undergoes a significant 2.5 Å positional shift toward Glu377.[57] This pivotal observation uncovers a crucial structural secret: the IMiD-binding pocket is not a restrictive, rigid cavity, but rather harbors pre-existing permissive space that allows for ligand movement. Such inherent plasticity is essential for accommodating the subtle structural rearrangements required to facilitate optimal protein-protein interactions.

Inspired by the existence of this navigable spatial volume, and leveraging our expertise in light-induced primary amine and o-nitrobenzyl alcohol cyclization (PANAC) chemistry,[58-64] we envisioned that the indazolone-based architecture—a product of PANAC photoclick chemistry—could serve as a promising structural platform for designing next-generation CRBN binders (Figure 2b). Central to our design is the intrinsic N-substitutability of the indazolone framework, which provides a highly tunable

structural template. Unlike the rigid classic isoindolinone scaffold, this optimizable platform allows for the precise installation of functional groups to strategically occupy and exploit the movable space identified by the 2.5 Å shift (Figure 2a). By fine-tuning these N-substituents, we aim to move beyond the traditional isoindolinone paradigm, exploring untapped chemical space to achieve superior geometric complementarity and enhanced neo-substrate recruitment (Figure 1b).

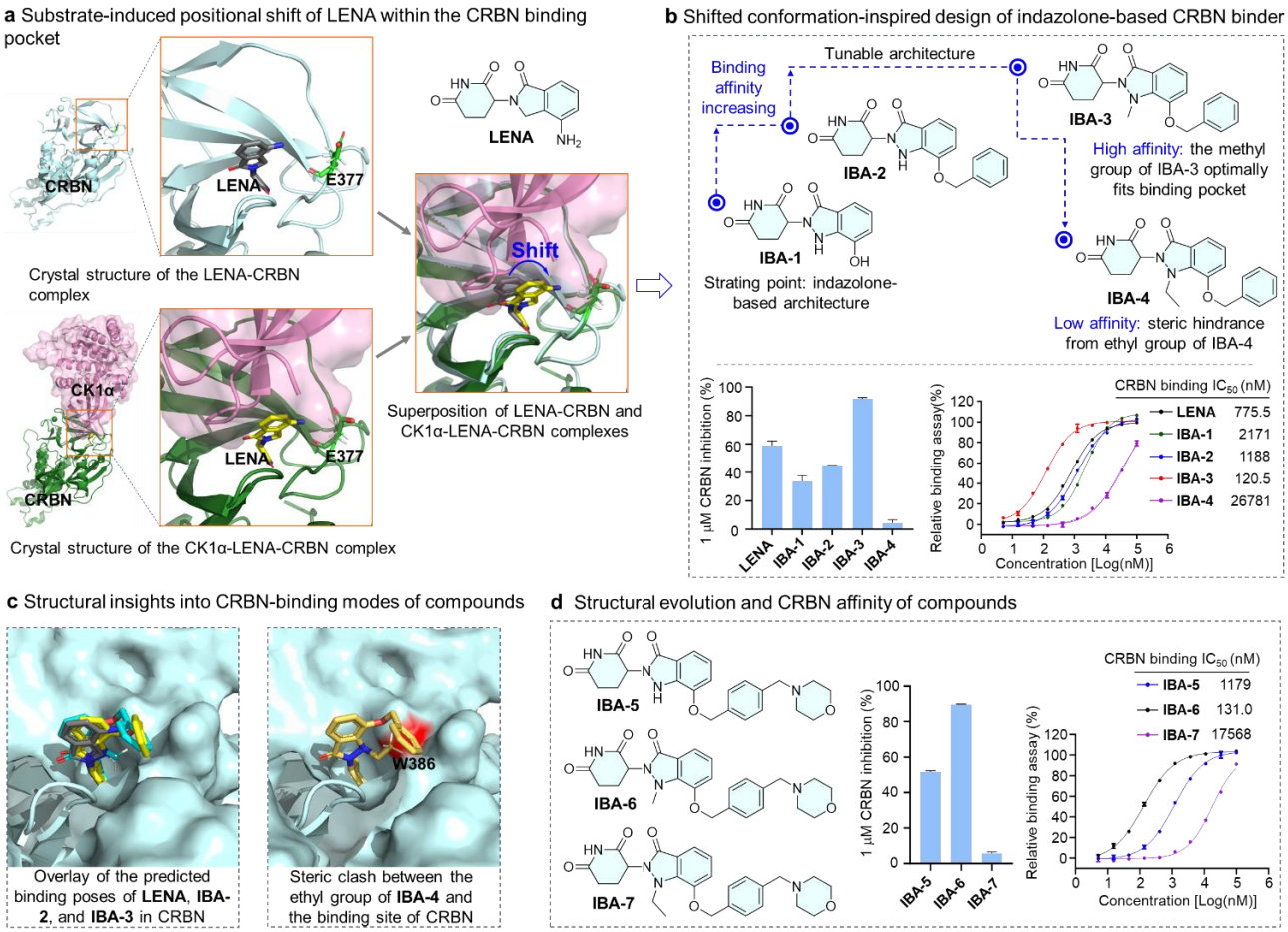

Figure 2. Establishment of a tunable indazolone-based architecture platform for MGDs discovery. a) Overlay of the crystal structures of the LENA-CRBN complex (PDB ID: 4TZ4) and the CK1α-LENA-CRBN complex (PDB ID: 5FQD), upon recruitment of the neo-substrate CK1α, LENA undergoes a significant 2.5 Å positional shift toward Glu377. **b)** Chemical structures of designed tunable indazolone derivatives (**IBA-1** to **IBA-4**) with various N-substituents. Evaluation of the relative CRBN binding affinities of lenalidomide and compounds **IBA-1** to **IBA-4** using a TR-FRET assay, displaying the relative inhibition at 1 μM, and IC_{50} values of compounds. Data represent mean ± SD (n = 2 biologically independent samples). **c)** Molecular docking poses of the synthesized compounds. The left panel shows the overlay of **LENA** (gray), **IBA-2** (yellow), and **IBA-3** (cyan) within the CRBN pocket (PDB ID: 4TZ4). The right panel displays the predicted position of the N-ethyl group of **IBA-4** within the CRBN binding site. **d)** Chemical structures of compounds **IBA-5** to **IBA-7**. Assessment of their relative CRBN binding affinities via TR-FRET analysis, detailing the percent inhibition at 1 μM and the IC_{50} values of compounds. Data represent mean ± SD (n = 2 biologically independent samples).

Driven by this hypothesis, we synthesized compounds **IBA-1** and **IBA-2** (Figure 2b). Then, we employed a TR-FRET CRBN binding assay to assess the relative binding affinities. To our delight, when evaluated for CRBN inhibition at a concentration of 1 μM, these indazolone-based architectures exhibited binding affinities comparable to that of **LENA**. This initial result strongly indicated that the indazolone scaffold could serve as a promising CRBN ligand. To further explore this, we synthesized compound **IBA-3** by introducing a methyl substituent at the N-position of the indazolone core. Remarkably, this modification led to a substantial enhancement in binding capacity (91% inhibition for **IBA-3** vs. 59% for **LENA**) (Figure 2b). Subsequent IC_{50} determinations revealed that **IBA-3** achieved a binding affinity of 120 nM, representing a more than 6-fold improvement over **LENA** (120 nM vs. 776 nM). Furthermore, to probe the spatial limits, we introduced a bulkier ethyl group at the nitrogen atom (**IBA-4**), which resulted in an almost complete loss of CRBN binding affinity ($IC_{50} > 26$ μM). To rationalize these divergent structure-activity relationships, we performed molecular docking analyses of these compounds with CRBN (Figure 2c). The predicted binding poses revealed that these indazolone derivatives share a binding mode highly similar to that of **LENA** observed in the crystal structure, successfully overlaying within the pocket. Together, the experimental data and computational predictions suggest that the N-methyl group of **IBA-3** optimally exploits the pre-existing permissive space within the CRBN binding pocket, thereby conferring high binding affinity. Conversely, the unsubstituted indazolone scaffolds (**IBA-1** and **IBA-2**) display comparable binding affinities to LENA due to their similar steric bulk to the classic isoindolinone scaffold. However, the introduction of the ethyl group in **IBA-4** induces severe steric clashes with Trp386 (Figure 2c, 2d), profoundly abrogating its ability to bind CRBN.

To further investigate whether increased structural complexity would compromise the CRBN-binding affinity of these indazolone-based architectures, we synthesized compounds **IBA-5** to **IBA-7** by incorporating a morpholinomethyl group onto the phenyl ring (Figure 2d). As anticipated, **IBA-5** (the unsubstituted derivative) exhibited a binding profile comparable to its corresponding analogue, **IBA-2** (Figure 2b and Figure 2c). Meanwhile, **IBA-6**, which bears an N-methyl substituent on the indazolone core, demonstrated robustly enhanced CRBN-binding activity, analogous to **IBA-3**. Conversely, the introduction of an N-ethyl group in **IBA-7** once again resulted in poor binding affinity, mirroring the behavior of **IBA-4**. Compellingly, these findings validate that our rationally designed indazolone-glutarimide architecture can serve as a robust next-generation CRBN binder. More importantly, the strategic introduction of a methyl group at the nitrogen atom yields a highly tunable architecture, offering a broader repertoire of choices for the design of CRBN-targeting MGDs.

This SAR trend was also reflected in the antiproliferative activity. The series showed selective activity in MM.1S cells, where **IBA-2**, **IBA-3**, **IBA-5**, and **IBA-6** inhibited cell proliferation with IC_{50}

values of 351.3, 160.1, 150.8, and 30.36 nM, respectively, whereas the N-ethyl analogues **IBA-4** and **IBA-7** were inactive (Table S1). Consistent with the CRBN-binding data, the N-methyl analogues **IBA-3** and **IBA-6** were more potent than their unsubstituted counterparts. In Mino cells, only **IBA-2** and **IBA-5** showed measurable activity (IC_{50} = 9044 and 2377 nM, respectively), while all compounds were inactive in MV-4-11 cells (Table S1). Rat liver microsomal stability further differentiated this series: **IBA-2** showed moderate stability ($t_{1/2}$ = 25.5 min; Cl_{int} = 0.1361 mL/min/mg), whereas **IBA-3** was rapidly cleared ($t_{1/2}$ = 1.61 min; Cl_{int} = 2.146 mL/min/mg). In contrast, the morpholinomethyl-substituted analogues **IBA-5** ($t_{1/2}$ = 1095 min; Cl_{int} = 0.0032 mL/min/mg) and **IBA-6** ($t_{1/2}$ = 138 min; Cl_{int} = 0.0251 mL/min/mg) displayed improved stability, with long half-lives and low intrinsic clearance (Table S2). In addition, all compounds from IBA-2 to IBA-6 exhibited negligible hERG inhibition (IC_{50} > 40 μM), suggesting a favorable cardiac safety profile and supporting the drug-like potential of this scaffold. Taken together, these results demonstrate that increasing the molecular complexity based on either the unsubstituted or N-methylated indazolone scaffolds does not compromise productive CRBN engagement and can be accompanied by favorable cellular activity and metabolic stability. This feature is of paramount importance, as it successfully unlocks novel chemical space for our subsequent development of MGDs with much greater structural diversity built upon these two privileged scaffolds.

Discovery of Indazolone-Based MGD Targeting Diverse Neo-Substrates

Mechanistically, CRBN-mediated molecular glue degraders (MGDs) function by anchoring to the CRBN E3 ligase, thereby forming a neomorphic PPI interface that recruits neo-substrates harboring recognition motifs such as canonical G-loops or G-loop–like features. To guide the design of MGDs, recent structural and mechanistic studies in the field have conceptualized a prevailing model that partitions the MGD into a conserved core and a tunable extended region. In this established paradigm, the MGD core must preserve essential interactions within the IMiD-binding pocket while maintaining a compatible geometric shape to accommodate the incoming degrons. Beyond this core, the extended region serves as the primary determinant of the degradation profile. Structural modifications within this extended space—ranging from single-atom substitutions to more complex molecular expansions—synergistically dictate target selectivity and stabilize the neomorphic PPI interface, thereby simultaneously modulating substrate preference and overall binding potency. Building on this field-wide framework, we recognized that our indazolone-based architectures inherently satisfy the restrictive requirements of the CRBN-binding core, while offering versatile substitution vectors to strategically access and tune this critical extended region. Driven by this rationale, in the subsequent sections, we designed and synthesized a variety of structurally more complex molecular glue degraders based on the unsubstituted or N-methylated indazolone scaffolds.

Having established the indazolone–glutarimide scaffold as a robust CRBN-binding architecture with tunable substitution vectors, we next sought to determine whether this newly developed platform could be leveraged to induce neo-substrate recruitment and targeted protein degradation. To this end, we designed compound **IBA-8** by extending the **IBA-5** scaffold through replacement of the morpholine moiety with a piperazine linker and incorporation of a substituted aromatic group (Figure 3a). This structural elaboration was intended to probe the accessible interaction space surrounding the CRBN pocket and evaluate whether the indazolone architecture could function as a molecular glue degrader capable of engaging diverse neo-substrates.

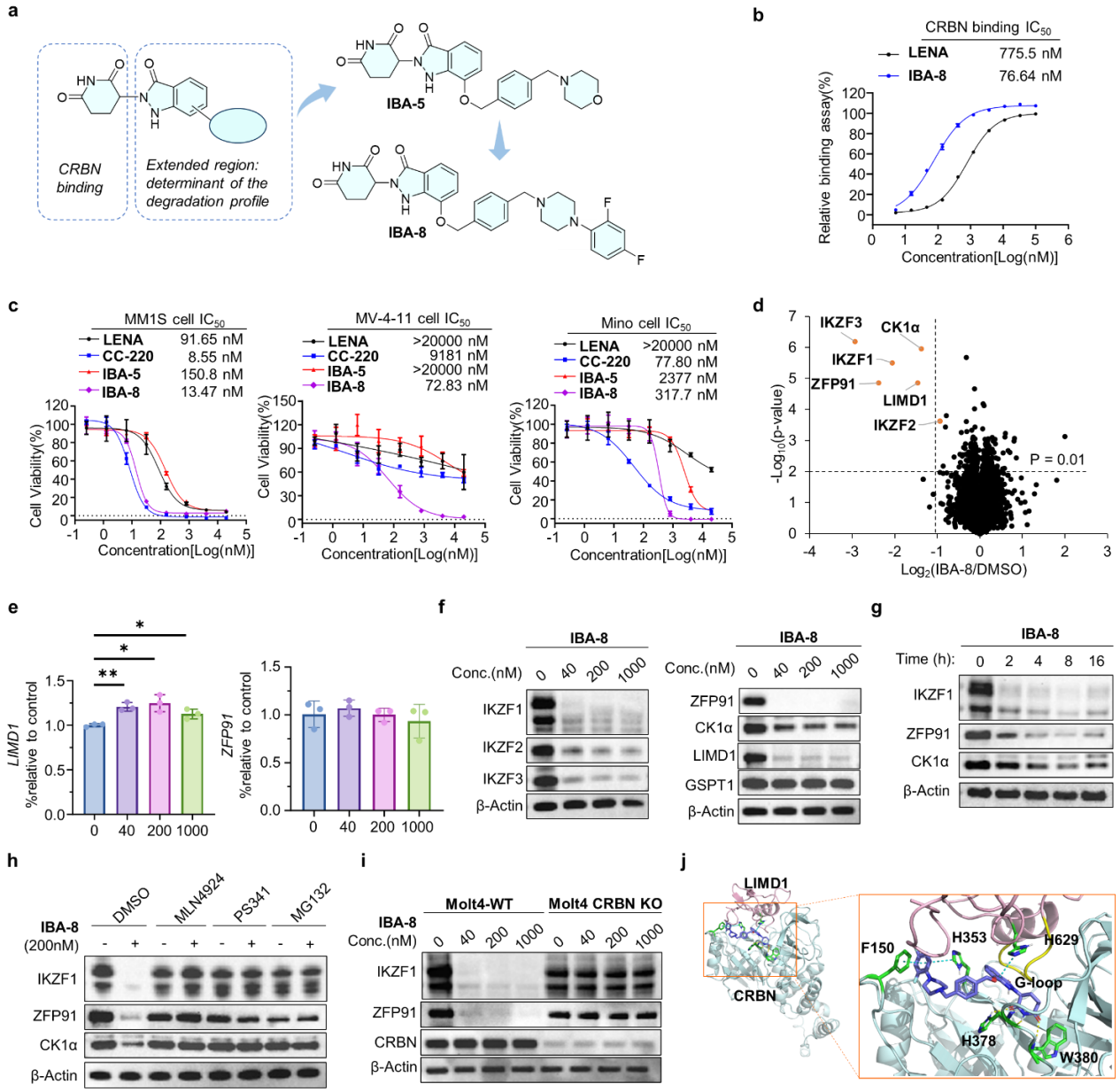

Figure 3. Discovery, mechanistic characterization, and diverse neo-substrate degradation profile of the indazolone-based molecular glue IBA-8. a) Chemical structures of **IBA-8**. **b)** Relative CRBN binding affinities of lenalidomide and **IBA-8** determined by TR-FRET. Data represent mean ± SD (n = 2 independent replicates). **c)** Cell viability assay of **IBA-8** in MM.1S, Mino, and MV-4-11 cells. Data are presented as mean ±SD, (n = 3 independent

replicates). IC_{50} values were calculated using the nonlinear fit variable slope model in GraphPad Prism 10. **d)** Global proteomic profiling in Mino cells treated with **IBA-8** at 200 nM for 4 h. Significant enrichment: Log_2 (**IBA-8**/DMSO) < -1 and p-value < 0.01, n = 3. **e)** Quantitative PCR analysis of mRNA expression of *LIMD1* and *ZFP91* in Mino cells treated with DMSO and **IBA-8** (40, 200, 1000 nM) for 8 h. P values were calculated using two-tailed t-test; *p<0.05, **p<0.01. **f)** Western blot analysis of the concentration-dependent degradation of IKZF1, IKZF2, IKZF3, ZFP91, LIMD1, CK1α, and GSPT1 in Mino cells treated with the various concentrations of **IBA-8** for 8 h. **g)** Immunoblot analysis of the time-dependent degradation of IKZF1, CK1α, and ZFP91 in Mino cells treated with 200 nM **IBA-8** for various durations. **h)** Mechanistic investigation of target degradation. Mino cells were pretreated with DMSO, MLN4924 (0.5 μM), PS341 (1 μM), or MG132 (10 μM) for 2 h, followed by treatment with 200 nM **IBA-8** for 3 h. Protein levels of IKZF1, ZFP91, and CK1α were subsequently evaluated by immunoblotting. **i)** Western blot analysis of IKZF1 and ZFP91 in wild type Molt4 cells and $CRBN^{-/-}$ Molt4 cells treated with **IBA-8**. **j)** Docking model of the CRBN (cyan): **IBA-8** (light blue): LIMD1 (lightpink) ternary complex. **IBA-8** was docked into the CRBN crystal structure (PDB ID: 4TZ4) using Schrödinger 2025-2, followed by protein–protein docking with the predicted structure of LIMD1 (AlphaFold, UniProt ID: Q9UGP4). LIMD1with β-hairpin G-loop predictions (yellow).

To evaluate its ability to engage CRBN, we measured the binding affinity using a TR-FRET assay. **IBA-8** exhibited potent binding activity with an IC_{50} of 76.64 nM (Figure 3b), demonstrating an approximately 10-fold enhancement in affinity compared with lenalidomide (IC_{50} = 775.5 nM). In antiproliferative assays, **IBA-8** showed markedly improved cellular activity over **IBA-5** and lenalidomide, and displayed greater potency than CC-220 in MV-4-11 cells (Figure 3c). **IBA-8** inhibited MM.1S, MV-4-11, and Mino cells with IC_{50} values of 13.47, 72.83, and 317.7 nM, respectively (Figure 3c). These data indicate that structural elaboration of the **IBA-5** scaffold to **IBA-8** substantially enhances cellular potency and broadens its antiproliferative profile.

Subsequently, to map the degradation landscape and identify specific targets, we performed Global proteomic profiling in Mino cells treated with **IBA-8**. Proteome-wide profiling revealed significant downregulation of several CRBN neosubstrates (Figure 3d), including IKZF1, IKZF3, CK1α, ZFP91, and LIMD1. Additional associated proteins, such as IKZF2, were also moderately depleted.. qPCR analysis after 8 h treatment in Mino cells showed that ZFP91 mRNA remained largely unchanged, whereas LIMD1 transcript levels modestly increased at 40 and 200 nM, indicating that the reduced protein levels were due to compound-induced degradation rather than transcriptional suppression (Figure 3e). Based on these findings, the identified substrates were selected for further validation and mechanistic investigation. Western blot analysis in Mino cells showed that **IBA-8** induced dose-dependent degradation of IKZF1, IKZF3, ZFP91, IKZF2, and LIMD1 after 8 h treatment, with substantial degradation evident at 40 nM (Figure 3f). By contrast, no degradation of GSPT1 was detected, and CK1α showed only partial loss at 1000 nM (Figure 3f), indicating a selective degradation profile. Time-course studies further showed rapid and near-complete degradation of IKZF1 and ZFP91 within 2-4 h at 200 nM, whereas CK1α degradation was slower and less efficient (Figure 3g).

To investigate the mechanism of action, we examined whether **IBA-8**-induced degradation depends on the ubiquitin–proteasome system. Degradation of IKZF1, ZFP91, CK1α, IKZF2 and LIMD1 was fully rescued by cotreatment with MLN4924 or the proteasome inhibitors PS341 and MG132 (Figure 3h and Figure S1a), indicating a CRL-dependent proteasomal mechanism. CRBN dependence was further confirmed in wild-type Molt4 cells and CRBN-knockout Molt4 cells, where **IBA-8**-induced IKZF1, ZFP91 and LIMD1 degradation was abolished in the absence of CRBN (Figure 3i and Figure S1b). Similarly, CK1α degradation was detected in wild-type but not CRBN-knockout HEK293T cells (Figure S1c), further supporting the CRBN-dependent activity of **IBA-8**. To further evaluate its metabolic stability, the microsomal stability of **IBA-**8 was assessed in rat liver microsomes. **IBA-8** exhibited a half-life ($t_{1/2}$) of 51.1 min and a low intrinsic clearance (Cl_{int} = 0.0678 mL/min/mg), indicating favorable metabolic stability.

To gain further insight into the structural basis of **IBA-8**-mediated LIMD1 degradation, we performed molecular docking studies to investigate the potential binding conformations of **IBA-8** with CRBN / ZFP91 within a ternary complex model. As shown in Figure 3j, consistent with the canonical binding mode of previously reported CRBN-recruiting molecular glues, the glutarimide ring of **IBA-8** occupies the tritryptophan pocket of CRBN. Notably, the 3-fluorobenzonitrile moiety of **IBA-8** forms π–π interactions with Phe150 and His353 of CRBN. In addition, the indazolone ring engages in a π–π interaction with the side chain of His629 from LIMD1 for added stability. The AlphaFold-predicted structure of LIMD1 contains a canonical β-hairpin G-loop degron that exhibits favorable surface complementarity to the CRBN-**IBA-8** interface, thereby enabling MGD-dependent recruitment and subsequent degradation. Collectively, these results demonstrate that **IBA-8** functions as a potent CRBN-dependent molecular glue degrader capable of inducing degradation of multiple neo-substrates, including IKZF1/3, ZFP91, LIMD1, IKZF2, and CK1α. This multi-target degradation profile highlights the capacity of the indazolone scaffold to generate diverse degradation outcomes, providing the first evidence that this platform can effectively reprogram the CRBN degradome.

Structural Refinement of Indazolone-Based MGDs to Reprogram CRBN Substrate Selectivity

Although **IBA-8** demonstrated potent degradation activity toward multiple CRBN neo-substrates, its broad degradation profile also included LIMD1, a well-recognized tumor suppressor protein.[65-67] The degradation of such proteins may introduce potential safety concerns and therefore underscores the importance of reprogramming substrate selectivity within the indazolone scaffold. We therefore next sought to determine whether subtle structural modifications could redirect the degradation landscape.

Guided by this rationale, structure-guided optimization of **IBA-8** led to the design of **IBA-9**, in which modifications to the indazolone ring and side-chain substitution pattern were introduced to remodel the CRBN–substrate interaction interface (Figure 4a). In a TR-FRET assay, **IBA-9** retained strong CRBN engagement with an IC_{50} of 115.3 nM, representing a ~7-fold improvement over lenalidomide (IC_{50} = 775.5 nM) (Figure 4b). Consistent with this, **IBA-9** exhibited potent antiproliferative activity in hematological malignancy cell lines, including MM.1S (IC_{50} = 28.68 nM), Mino (IC_{50} = 91.19 nM), and MV-4-11 cells (IC_{50} = 72.45 nM) (Figure 4c).

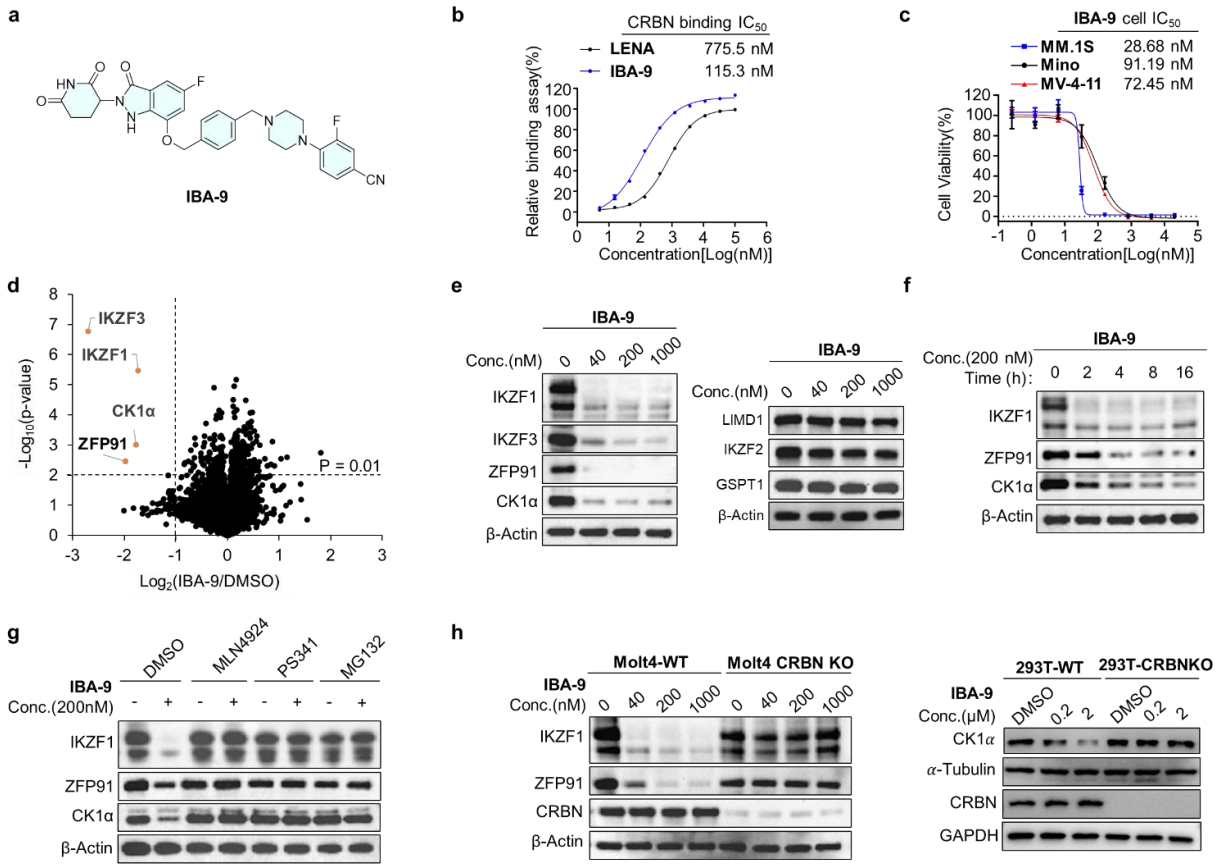

Figure 4. Identification of MGD IBA-9 and validation of its programmable neo-substrate degradation. a) Chemical structure of **IBA-9**. **b)** TR-FRET-based evaluation of relative CRBN binding affinities for LENA and **IBA-9**. Date are shown as mean ± SD (n=2 independent replicates). **c)** Anti-proliferative activity of **IBA-9** against MM.1S, Mino, and MV-4-11 cell lines. Date are shown as mean ± SD (n = 3 independent replicates), with IC_{50} values derived via a nonlinear fit variable slope model (GraphPad Prism 10). **d)** Proteomic analysis of Mino cells following treatment with 200 nM **IBA-9** for 4 h. Thresholds for significant protein alterations were set at Log_2 fold change (**IBA-9**/DMSO) < -1 and p-value < 0.01 (n = 3). **e)** Immunoblotting assessment of concentration-dependent degradation (IKZF1, IKZF3, ZFP91, CK1α, GSPT1, IKZF2, and LIMD1) in Mino cells exposed to various doses of **IBA-9** for 8 h. **f)** Time-dependent degradation profiles of IKZF1, CK1α, and ZFP91 in Mino cells incubated with 200 nM **IBA-9**. **g)** Rescue of **IBA-9**-induced CK1α degradation by pretreatment with MLN4924 (0.5 μM), PS341 (1 μM), or MG132 (10 μM) for 2 h, followed by treatment with 200 nM **IBA-9** for 3 h in Mino cells. **h)** WB analysis of IKZF1 and ZFP91 in wild type Molt4 cells and $CRBN^{-/-}$ Molt4 cells following treatment with **IBA-9** (left); WB analysis of CK1α in wild-type (WT) and $CRBN^{-/-}$ HEK293T cells following treatment with **IBA-9** (right).

To identify substrates targeted by **IBA-9**, we conducted quantitative proteomic profiling in Mino cells. Proteome-wide analysis revealed a selective degradation signature (Figure 4d), with significant downregulation of multiple neosubstrates, most prominently IKZF1, IKZF3, CK1α, and ZFP91. Notably, the degradation profile differed from that of **IBA-8**, indicating that the introduced structural modifications reshaped substrate selectivity and reprogrammed CRBN-mediated recognition. These proteins were therefore prioritized for subsequent validation and mechanistic studies.

Western blot analysis confirmed that **IBA-9** induced robust, dose-dependent degradation of IKZF1, IKZF3, ZFP91 and CK1α following 8 h treatment in Mino cells, with clear effects observed at concentrations as low as 40 nM (Figure 4e). In contrast, GSPT1, IKZF2, and LIMD1 showed minimal or no degradation even at concentrations up to 1 μM, indicating improved substrate selectivity relative to **IBA-8**. Time-course experiments revealed rapid degradation kinetics, with treatment of Mino cells with 200 nM **IBA-9** leading to near-complete depletion of IKZF1 within 2 h (Figure 4f), while CK1α and ZFP91 were substantially degraded by 4 h and nearly completely depleted by 16 h.

To clarify the mechanism, we tested whether degradation depends on the ubiquitin–proteasome system. Co-treatment with the MLN4924 or PS341 and MG-132 fully blocked degradation (Figure 4g), demonstrating reliance on the ubiquitin–proteasome system. Consistently, degradation of IKZF1 and ZFP91 was observed in wild-type Molt4 cels but completely abolished in CRBN-knockout Molt4 cells. Likewise, CK1α degradation was detected in wild-type HEK293T cells but not in CRBN-knockout cells (Figure 4h), confirming the CRBN dependence. In addition, **IBA-9** displayed excellent metabolic stability in rat liver microsomes, with an apparent half-life exceeding the assay time window and negligible intrinsic clearance (Table S1). Taken together, these results demonstrate that subtle structural refinement of the indazolone scaffold can effectively reprogram the CRBN degradome. Compared with the broad substrate spectrum of **IBA-8**, **IBA-9** exhibits a more refined degradation profile that eliminates LIMD1 degradation while maintaining potent activity toward canonical substrates such as IKZF1/3 and ZFP91. These findings highlight the programmable nature of the indazolone platform and establish a foundation for further tuning substrate selectivity.

Rational Tuning of Indazolone-Based MGDs for High-Affinity CRBN Engagement and Refined Selectivity

Encouraged by the ability of **IBA-9** to reshape the degradation profile relative to **IBA-8**, we next explored whether the indazolone scaffold could be further tuned to achieve more precise control over substrate selectivity. Guided by this strategy, we introduced an N-methyl substitution on the indazolone core to enhance CRBN engagement, resulting in the design of **IBA-10** (Figure 5a). This modification

was anticipated to further refine the CRBN–substrate interface and modulate the degradation preference. In a TR-FRET binding assay, **IBA-10** showed strong CRBN binding (IC_{50} = 16.6 nM), representing a 47-fold improvement over lenalidomide (IC_{50} = 775.5 nM) (Figure 5b). We next assessed the antiproliferative activity of **IBA-10** across hematological malignancy cell lines (Figure 5c). **IBA-10** demonstrated strong growth inhibition, with IC_{50} values of 0.86 nM in MM.1S cells and 8.23 nM in Mino cells. This differential sensitivity suggests that **IBA-10** may induce selective neosubstrate degradation in a cell-context-dependent manner.

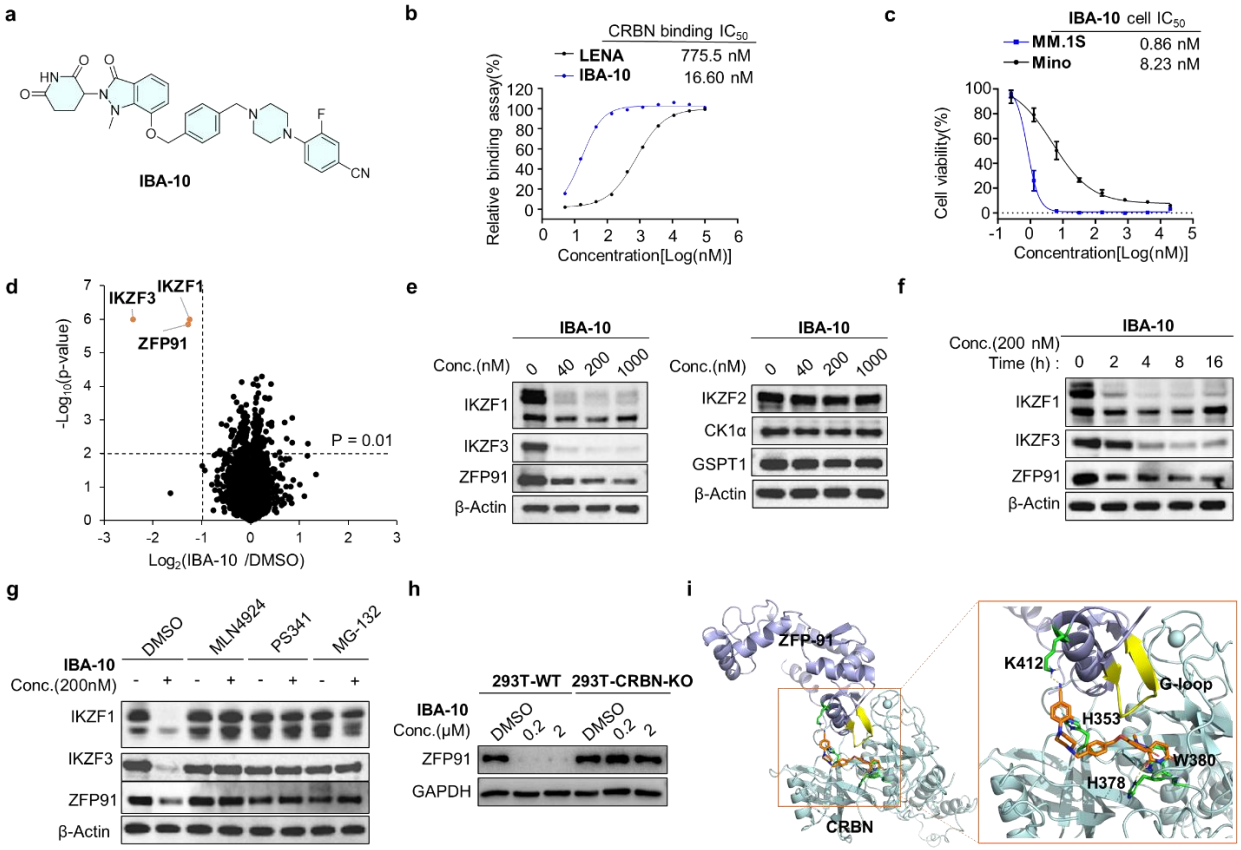

j

IBA-10	Dose(mg/kg)	$T_{1/2}$ (h)	T_{max} (h)	C_{max} (ng/mL)	AUC_{0-t} (h·ng/mL)	V_{ss} (L/kg)	CL (mL/min/kg)	$MRT_{0-\infty}$ (h)	F(%)
IV	2	2.68	0.194	1393	3748	1.27	8.87	2.39	
PO	10	2.49	0.667	2540	8339	/	/	2.57	44.5

Figure 5. Identification of the indazolone-based MGD IBA-10 and evaluation of its substrate selectivity. a) Chemical structure of **IBA-10**. **b)** TR-FRET-based evaluation of relative CRBN binding affinities for LENA and **IBA-10**. Date are shown as mean ± SD (n = 3 independent replicates). **c)** Cell growth inhibition profiles of **IBA-10** in MM.1S and Mino cells. Data represent the mean ± SD (n = 3 independent replicates). **d)** Proteomic analysis of Mino cells following treatment with 200 nM **IBA-10** for 4 h. **e)** Western blot evaluation illustrating the dose-dependent degradation of multiple CRBN substrates in Mino cells treated with the indicated concentrations of **IBA-10** for 8 h. Thresholds for significant protein alterations were set at Log_2 fold change (**IBA-10**/DMSO) < -1 and p-value < 0.01 (n = 3). **f)** Time-dependent degradation profiles of IKZF1, CK1α, and ZFP91 in Mino cells incubated with 200 nM **IBA-10** for various time intervals. **g)** Rescue of **IBA-10**-induced IKZF1/3 and ZFP91 degradation by pretreatment with MLN4924 (0.5 μM), PS341 (1 μM), or MG132 (10 μM) for 2 h, followed by treatment with 200 nM **IBA-10** for

3 h in Mino cells. **h)** Western blot analysis of CK1α in wild-type (WT) and CRBN$^{-/-}$ HEK293T cells treated with **IBA-10**. **i)** Docking binding model of CRBN (cyan): **IBA-10** (yellow): ZFP91 (light blue) complex. **IBA-10** was docked into the CRBN crystal structure (PDB ID: 4TZ4) using Schrödinger 2025-2, followed by protein–protein docking with the predicted structure of ZFP91 (AlphaFold, UniProt ID: Q96JP5). ZFP91 with β-hairpin G-loop predictions (yellow). **j)** PK Parameters of Compound **IBA-10** in Rats.

To characterize the degradome induced by **IBA-10**, quantitative proteomic profiling was performed in Mino cells. Proteome-wide analysis revealed selective downregulation of CRBN substrates, including IKZF1, IKZF3, and ZFP91 (Figure 5d). Western blot analysis confirmed dose-dependent degradation of IKZF1 and IKZF3 after 8 h treatment, with substantial depletion at 40 nM, whereas ZFP91 degradation required higher concentrations (1 μM) (Figure 5e). CK1α, GSPT1, and IKZF2 remained largely unaffected up to 1 μM. Time-course experiments showed rapid degradation of IKZF1 and IKZF3 within 2–4 h, reaching near-complete depletion by 8 h, while ZFP91 degradation was only detectable after 16 h (Figure 5f). Mechanistically, degradation was abolished by MLN4924, PS341, or MG132 and was absent in CRBN-knockout HEK293T cells, confirming a CRBN-dependent ubiquitin–proteasome mechanism (Figure 5h).

To gain structural insight into ZFP91 recruitment, molecular docking was performed to model the CRBN–**IBA-10**–ZFP91 ternary complex. As shown in Figure 5i, the glutarimide moiety of **IBA-10** occupies the canonical tri-tryptophan pocket of CRBN. The 3-fluorobenzonitrile group forms a π–π interaction with His353 of CRBN, while the cyano group establishes a hydrogen-bond interaction with Lys412 of ZFP91. ZFP91 is predicted to engage the CRBN–**IBA-10** interface through a β-hairpin G-loop. **IBA-10** also displayed good metabolic stability in rat liver microsomes, with a half-life ($t_{1/2}$) of 58 min and a low intrinsic clearance (Cl_{int} = 0.0599 mL/min/mg).We then evaluated the pharmacokinetic (PK) properties of **IBA-10** in rats(Figure 5j). **IBA-10** exhibited low systemic clearance (CL = 8.87 mL/min/kg) and a moderate steady-state volume of distribution (V_{ss} = 1.27 L/kg), with a terminal half-life ($t_{1/2}$) of 2.68 h and a mean residence time ($MRT_{0-\infty}$) of 2.39 h. Following oral administration at 10 mg/kg, **IBA-10** was rapidly absorbed with a T_{max} of 0.667 h and achieved a C_{max} of 2540 ng/mL. The compound displayed a half-life of 2.49 h and an $MRT_{0-\infty}$ of 2.57 h. The systemic exposure reached an AUC_{0-t} of 8339 h·ng/mL, corresponding to an oral bioavailability (F) of 44.5%. Overall, these results demonstrate that structural optimization of the indazolone scaffold can progressively refine the degradation landscape. Compared with the broader activity observed for **IBA-8** and **IBA-9**, **IBA-10** exhibits a more focused degradation profile primarily targeting IKZF1/3 and ZFP91, illustrating that the indazolone architecture enables stepwise tuning of CRBN substrate selectivity.

Discovery of an Indazolone-Based Molecular Glue for Highly Selective CK1α

Having demonstrated that the indazolone scaffold allows progressive modulation of substrate preference, we next sought to determine whether this platform could be further engineered to enable highly selective degradation of alternative CRBN neo-substrates. To test this possibility, we designed **IBA-11** by introducing a rigid aryl-substituted N-methylimidazole moiety at the C3 position of the indazolone core, with the aim of reshaping the solvent-exposed region and promoting recruitment of distinct substrates (Figure 6a).The binding affinity to CRBN was evaluated using a TR-FRET assay (Figure 6b). **IBA-11** exhibited moderate CRBN binding (IC_{50} = 2285 nM), representing reduced affinity relative to lenalidomide (IC_{50} = 775.5 nM).

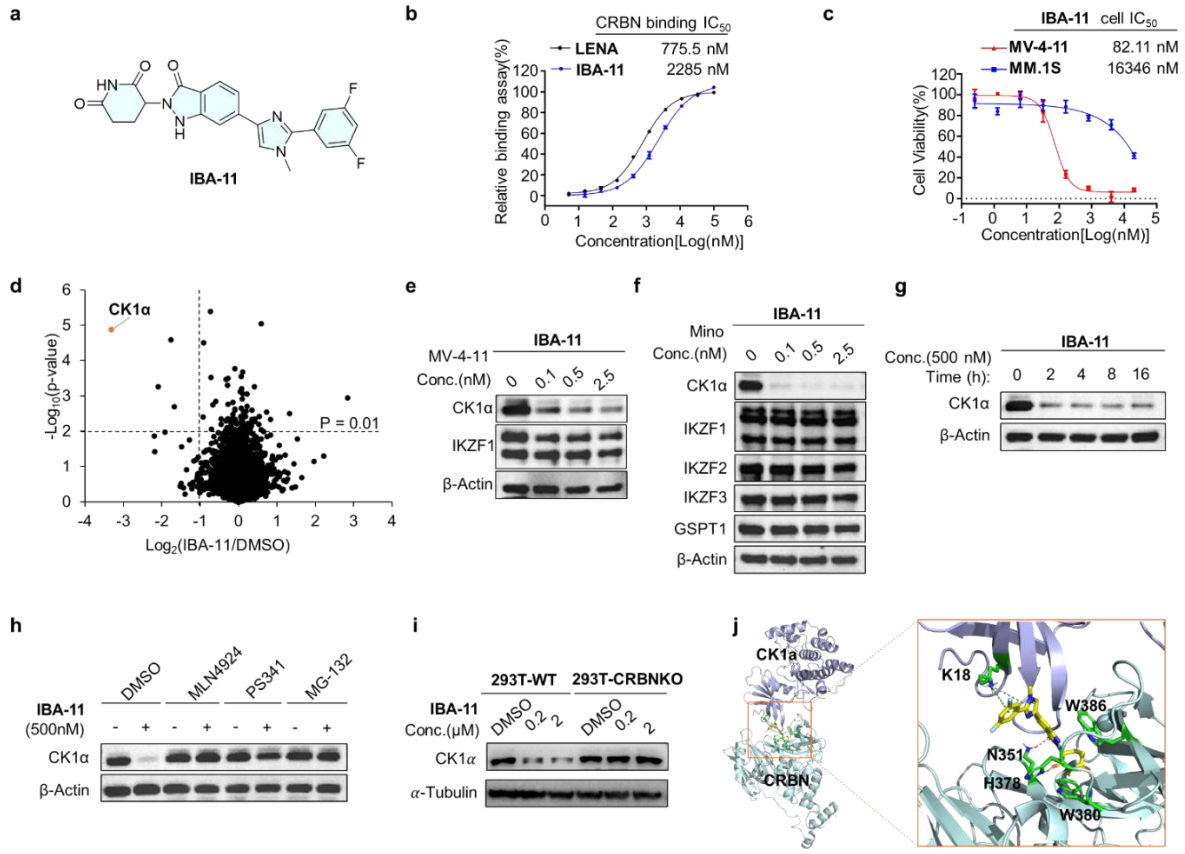

Figure 6. Discovery of the MGD IBA-11 and validation of selective CK1α degradation. a) Chemical structure of **IBA-11**. **b)** Assessment of the relative CRBN binding affinities of LENA and **IBA-11** via TR-FRET assay. Data are expressed as mean ± SD (n = 2 independent replicates). **c)** Cell growth inhibition profiles of **IBA-11** in MV-4-11 and MM.1S cells. Data represent the mean ± SD (n = 3 independent replicates). **d)** proteomic analysis of Mino cells following treatment with 200 nM **IBA-11** for 4 h. Thresholds for significant protein alterations were set at Log_2 fold change (**IBA-11**/DMSO) < -1 and p-value < 0.01 (n = 3). **e)** Western blot analysis of CK1α and IKZF1 in MV-4-11 cells treated with the indicated concentrations of **IBA-11** for 8 h. **f)** The dose-dependent degradation of multiple CRBN substrates in Mino cells treated with the indicated concentrations of **IBA-11** for 8 h. **g)** Time-dependent degradation profiles of CK1α in Mino cells incubated with 500 nM **IBA-11**. **h)** Rescue of **IBA-11**-induced CK1α degradation by pretreatment with MLN4924 (0.5 μM), PS-341 (1 μM), or MG-132 (10 μM) for 2 h, prior to an additional 3h exposure

to **IBA-11** (500nM), and subsequently analyzed by immunoblotting. **h)** Western blot analysis of CK1α in wild-type (WT) and CRBN$^{-/-}$ HEK293T cells treated with **IBA-11**. **j)** Docking of **IBA-11** with CRBN and CK1α. Predicted binding mode and interactions of CRBN (cyan): **IBA-11** (yellow): CK1α (lightblue) complex (PDB:5FQD).

We next assessed the antiproliferative activity of **IBA-11** across hematologic malignancy cell lines. While negligible growth inhibition was observed in MM.1S cells, **IBA-11** displayed potent cytotoxicity in MV-4-11 cells (IC_{50} = 82.11 nM) (Figure 6c). This divergent phenotypic profile suggested the possibility of context-dependent neosubstrate degradation. To identify potential targets, Proteome-wide profiling was performed in Mino cells, which revealed CK1α as the most significantly downregulated protein (Figure 6d).Western blot analysis further confirmed that **IBA-11** induced dose-dependent degradation of CK1α in both MV-4-11 and Mino cells following 8 h treatment, while IKZF1/2/3 and GSPT1 remained largely unaffected, indicating high substrate selectivity (Figure 6e,f). Time-course experiments revealed rapid degradation kinetics, with 500 nM **IBA-11** inducing near-complete CK1α depletion within 2 h (Figure 6g). Mechanistically, CK1α degradation was abolished by pretreatment with MLN4924, PS341, or MG132, indicating dependence on the ubiquitin–proteasome system (Figure 6h). Consistently, **IBA-11** induced concentration-dependent CK1α degradation in wild-type HEK293T cells but not in CRBN-knockout cells, confirming CRBN dependency (Figure 6i).

To gain structural insight into CK1α recruitment, molecular docking was performed based on the reported CRBN–CK1α crystal structure (PDB ID: 5FQD) (Figure 6j). The glutarimide moiety of **IBA-11** occupies the canonical tri-tryptophan pocket of CRBN (W380, W386, W400), while the isoindolinone core forms hydrogen-bond interactions with N351 and H378. In addition, Lys18 of CK1α engages in cation-π interactions with both the fluorophenyl ring and the imidazole moiety of **IBA-11**, potentially stabilizing the ternary complex and facilitating CK1α recruitment. **IBA-11** also displayed excellent metabolic stability in rat liver microsomes, with a half-life ($t_{1/2}$) of 184 min and a low intrinsic clearance (Clint = 0.0189 mL/min/mg), and exhibited minimal hERG inhibition (IC_{50} > 40 μM). Collectively, these findings establish **IBA-11** as a highly selective CK1α MGD, demonstrating that the indazolone scaffold can be engineered to selectively recruit individual CRBN neo-substrates. This result further underscores the versatility of this platform for generating degraders with distinct and programmable target profiles.

Discovery of IBA-12: A Potent Indazolone-Based MGD for Selective IKZF2 Degradation and *In Vivo* Antitumor Therapy

Building upon the programmable substrate selectivity observed for the indazolone scaffold, we next investigated whether this platform could be further optimized to achieve highly selective degradation of IKZF2, a therapeutically relevant target involved in immune regulation. Through rational

structural modification, introduction of a 1-(3-chlorobenzyl)piperidin-4-yl substituent led to the development of **IBA-12**, designed to favor recruitment of IKZF2 while minimizing degradation of other canonical CRBN substrates (Figure 7a).The binding affinity of **IBA-12** toward CRBN was evaluated using a TR-FRET assay. **IBA-12** exhibited strong CRBN binding (IC_{50} = 179.9 nM), representing a substantial improvement compared with lenalidomide (IC_{50} = 775.5 nM) (Figure 7b).

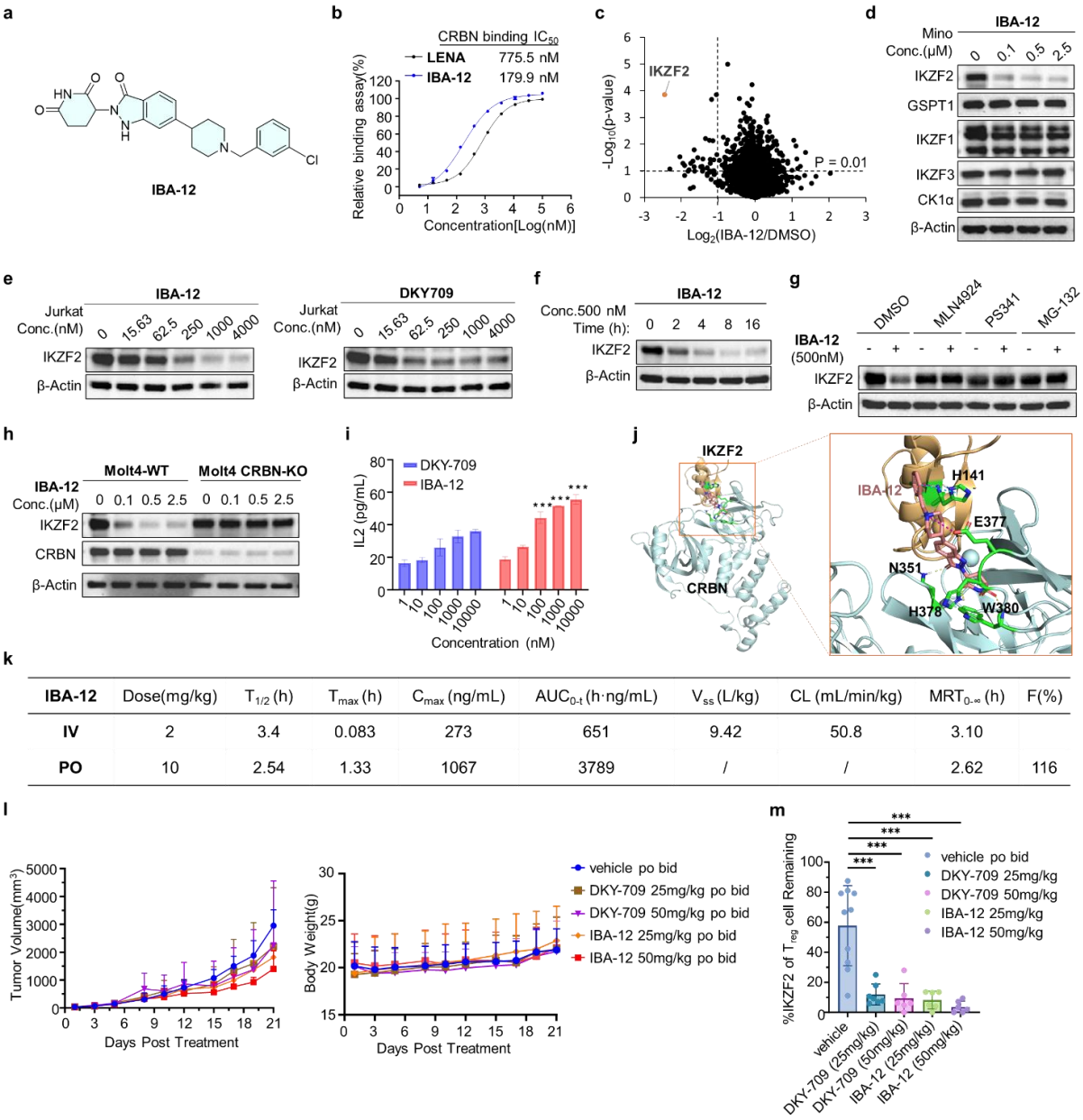

IBA-12	Dose(mg/kg)	$T_{1/2}$ (h)	T_{max} (h)	C_{max} (ng/mL)	AUC_{0-t} (h·ng/mL)	V_{ss} (L/kg)	CL (mL/min/kg)	$MRT_{0-\infty}$ (h)	F(%)
IV	2	3.4	0.083	273	651	9.42	50.8	3.10	
PO	10	2.54	1.33	1067	3789	/	/	2.62	116

Figure 7. Biological characterization of the IKZF2-selective molecular glue IBA-12. a) Chemical structure of **IBA-12**. **b)** CRBN binding affinities of LENA and **IBA-12** determined by TR-FRET assay. Data are expressed as mean ± SD (n = 2 independent replicates). **c)** Proteomic analysis of Mino cells following treatment with 1 μM **IBA-12** for 8 h. Thresholds for significant protein alterations were set at Log_2 fold change (**IBA-12**/DMSO) < -1 and p-value < 0.01 (n = 3). **d)** Western blot analysis of multiple CRBN substrates in Mino cells treated with the indicated concentrations of **IBA-12** for 8 h. **e)** Western blot analysis of IKZF2 levels in Jurkat cells treated with the indicated concentrations of **IBA-12** for 24 h. **f)** Time-dependent degradation profiles of IKZF2 in Mino cells treated with 500 nM IBA-12. **g)** Mino

cells were pretreated with MLN4924 (0.5 μM), PS341 (1 μM), or MG132 (10 μM) for 2 h prior to treatment with 0.5 μM **IBA-12** for 4 h. **h)** Western blot analysis of IKZF1 and ZFP91 in wild-type Molt4 cells and $CRBN^{-/-}$ Molt4 cells treated with **IBA-12**. **i)** Jurkat cells were stimulated with SEE-pulsed Raji cells in the presence or absence of DKY-709 or **IBA-12**. Culture supernatants were collected after 24 h and IL-2 production was quantified by ELISA. Data are presented as mean ± SEM (n = 3 biological replicates per concentration). "***" $P < 0.001$. **j)** Predicted binding mode of **IBA-12** (red) in complex with CRBN (cyan) and IKZF2 (wheat) based on molecular docking (PDB ID: 8DEY). **k)** Pharmacokinetic parameters of **IBA-12** in rats. **l)** Tumor growth inhibition induced by daily DKY-709 or **IBA-12** treatment (25 or 50 mg/kg) in the MC38 tumor model in $Crbn^{V380E/I391V}$ mice (left). Vehicle group, $n = 12$; treatment groups, $n = 6$. Body weight changes of mice during treatment (right). **m)** *In vivo* degradation of IKZF2 in peripheral Treg cells 2 h after the final oral administration of the indicated doses of DKY-709 or **IBA-12** in $Crbn^{V380E/I391V}$ mice.

To identify potential neosubstrates, quantitative proteomic profiling was performed. Proteome-wide analysis revealed IKZF2 as the most significantly and selectively downregulated protein (Figure 7c). Western blot analysis confirmed robust, dose-dependent IKZF2 degradation in Mino cells following 24 h treatment with **IBA-12**, with substantial depletion observed at 0.1 μM (Figure 7d). In contrast, classical CRBN substrates including GSPT1, IKZF1, IKZF3, and CK1α remained largely unchanged even at concentrations up to 2.5 μM, highlighting the high substrate selectivity of **IBA-12**. Quantification yielded a DC_{50} value of 461.8 nM, demonstrating improved degradation potency relative to the clinical IKZF2 degrader DKY-709 (DC_{50} = 1194 nM). Consistent results were observed in Jurkat cells, where **IBA-12** induced dose-dependent IKZF2 degradation after 24 h treatment (Figure 7e). Quantitative analysis gave a DC_{50} of 385.4 nM and D_{max} of 77.14%, representing improved degradation efficiency compared with DKY-709 (DC_{50} = 872.7 nM, D_{max} = 56.75%). Time-course experiments further revealed progressive IKZF2 degradation, with 500 nM **IBA-12** inducing marked protein loss between 4 and 8 h (Figure 7f).

Mechanistic studies showed that IKZF2 degradation was completely blocked by MLN4924 or the proteasome inhibitors PS341 and MG132 (Figure 7g), demonstrating dependence on CRL ligase activity and the ubiquitin–proteasome pathway. Consistently, degradation was observed in wild-type Molt4 cells but abolished in CRBN-knockout cells, confirming CRBN dependency (Figure 7h). IKZF2 has been reported to repress transcription of interleukin-2 (IL-2) in regulatory T cells.[68] Accordingly, treatment of Jurkat cells stimulated by with Raji cells (1:1) with **IBA-12** or DKY-709 resulted in dose-dependent increases in IL-2 production (Figure 7i), indicating functional modulation of an IKZF2-regulated transcriptional pathway.

To gain structural insight into **IBA-12**-mediated IKZF2 recruitment, molecular docking studies were performed using the reported IKZF2-CRBN crystal structure (PDB ID: 8DEY). As shown in Figure 7j, the glutarimide moiety of **IBA-12** occupies the canonical tri-tryptophan pocket of CRBN. The protonated nitrogen of the piperidine ring forms a salt bridge with Glu377 of CRBN, a feature also

observed in the IKZF2 degrader DKY-709.[36] At the CRBN–IKZF2 interface, **IBA-12** further establishes π–π stacking interactions with H141 together with an additional salt-bridge interaction, stabilizing the IKZF2–**IBA-12**–CRBN ternary complex. **IBA-12** also displayed favorable metabolic stability in rat liver microsomes, with no detectable metabolic turnover (Table S2).

IBA-12 showed excellent stability in rat liver microsomes, with no detectable metabolic turnover. We next evaluated the pharmacokinetic properties of **IBA-12** in rats (Figure 7k). **IBA-12** displayed moderate clearance (CL = 50.8 mL/min/kg), a large volume of distribution (Vss = 9.42 L/kg), and a half-life of 3.40 h. Oral administration (10 mg/kg) resulted in rapid absorption (T_{max} = 1.33 h), high exposure (AUC_{0-t} = 3789 h/ng/mL), and excellent oral bioavailability (F = 116%). Encouraged by these favorable properties, we next evaluated the *in vivo* antitumor efficacy of **IBA-12** using the MC38 syngeneic tumor model in humanized CRBN ($Crbn^{V380E/I391V}$) mice. Oral administration of DKY-709 or **IBA-12** (25 or 50 mg/kg, bid) for 21 days resulted in dose-dependent tumor growth inhibition (Figure 7l). Treatment with **IBA-12** at 50 mg/kg resulted in moderate tumor growth inhibition, slightly improved relative to DKY-709 under the same dosing regimen. **IBA-12** was well tolerated with no significant body weight loss (Figure 7l). Analysis of peripheral Treg cells 2 h after the final dose showed efficient IKZF2 degradation *in vivo*, slightly improved compared with DKY-709 (Figure 7m). Collectively, these results establish **IBA-12** as a potent and selective IKZF2 molecular glue degrader that promotes IKZF2 degradation through the $CRL4^{CRBN}$-dependent ubiquitin–proteasome pathway. Together with its favorable pharmacokinetic properties, efficient *in vivo* IKZF2 degradation, and antitumor activity in the MC38 tumor model, **IBA-12** represents a promising candidate for the development of next-generation IKZF2-targeted MGDs.

Broader Implications and Future Potential of the Indazolone-Based MGD Discovery Platform

MGD has rapidly transformed drug discovery, yet a significant challenge persists: the predominant reliance on a limited number of chemical scaffolds, notably the canonical isoindolinone glutarimide, for recruiting the E3 ligase CRBN. This over-reliance inadvertently constrains the exploration of the vast degradable proteome, limiting both chemical diversity and the scope of therapeutically relevant targets accessible to MGDs. In this context, the indazolone-based MGD discovery platform presented in this work represents a crucial advancement, offering an innovative paradigm that directly addresses these inherent limitations and paves the way for a next generation of MGDs with enhanced substrate programmability and therapeutic potential.

Our research first highlights a profound implication by successfully expanding the chemical space that has long challenged CRBN-MGD discovery. Our efforts demonstrate that the indazolone scaffold, a structurally distinct chemotype, serves as a highly effective CRBN binder. Through rigorous evaluation of compounds **IBA-1** to **IBA-7**, we have established this novel structural foundation for MGDs**,** dramatically expanding the chemical diversity available for modulating CRBN function. By moving beyond traditional scaffolds, our platform effectively broadens previously unexplored chemical space, which is critical for overcoming intrinsic architectural limitations and enabling access to a wider array of neo-substrates, thereby achieving superior pharmacological profiles.

The success of our platform is deeply rooted in design principles guided by mechanistic insights. We leveraged existing structural insights—the observed positional shift in the CRBN-LENA-CK1α complex—to inspire the rational design of the indazolone architecture. The intrinsic N-substitutability of the indazolone framework allows us to precisely occupy and strategically exploit this permissive space within the CRBN binding pocket. This strategy led to optimized binding affinities and, critically, differential neo-substrate recruitment. This structure-informed design approach represents a significant step forward, deepening our understanding of the structural principles governing MGD-E3-substrate ternary complex formation and providing a robust blueprint for future MGD scaffold engineering.

Crucially, this indazolone platform offers exceptional programmability of CRBN substrate specificity, addressing a central challenge in MGD development: the ability to precisely dictate which neo-substrate is recruited for degradation. Our results provide compelling evidence that subtle structural modifications within the indazolone scaffold lead to dramatic shifts in degradation profiles. We have systematically demonstrated how compounds such as **IBA-8**, **IBA-9**, **IBA-10**, **IBA-11**, and **IBA-12**, despite their structural kinship, elicit distinct and often highly selective degradation patterns. For instance, **IBA-8** functions as a potent multi-target degrader of IKZF1/3, CK1α, IKZF2, ZFP91, and LIMD1. Remarkably, modest structural refinements in **IBA-9** reprogram this profile, leading to a more selective degradation of IKZF1/3, CK1α, and ZFP91. Most strikingly, **IBA-12** achieved exquisite selectivity for IKZF2, without affecting other canonical CRBN substrates such as IKZF1/3 or GSPT1. This remarkable ability to fine-tune neo-substrate recognition through structural diversification establishes our indazolone platform as a powerful tool for developing MGDs to target new proteins of interest relevant to specific therapeutic needs.

The broad biomedical application potential of this platform is immense. By generating highly potent and selective degraders for therapeutically relevant targets such as IKZF1/3, ZFP91, CK1α, and IKZF2, our work directly addresses unmet medical needs in various diseases. For instance, the selective degradation of CK1α by **IBA-11** opens promising new avenues for therapy for acute myeloid leukemia (AML), while the highly specific IKZF2 degrader **IBA-12** holds significant promise for

immunomodulation and for treating hematological malignancies where precise targeting is critical. The ability to generate such diverse pharmacological profiles from a single, tunable scaffold family suggests that the indazolone platform can effectively expand the druggable proteome by converting previously "undruggable" proteins into tractable therapeutic targets, thereby offering novel therapeutic strategies for challenging diseases.

Looking forward, our indazolone-based MGD discovery platform offers a compelling vision for future MGD development. The remarkable tunability and demonstrated efficacy of the indazolone scaffold suggest significant potential for further rational optimization. This includes exploring additional substituent modifications, investigating stereochemical variations, and developing hybrid designs to achieve even finer control over substrate specificity and degradation efficiency. Continued efforts will also focus on deepening the mechanistic understanding of how specific structural features of indazolone MGDs dictate their unique degradation profiles, potentially through advanced structural biology techniques, such as co-crystal structures of indazolone MGDs with CRBN and their respective neo-substrates, to visualize ternary complex formation at atomic resolution. Moreover, the favorable pharmacokinetic properties observed for compounds like **IBA-10** and **IBA-12** highlight the platform's capacity to yield molecules suitable for further preclinical development. Future work will therefore prioritize comprehensively evaluating and optimizing the PK/PD profiles of lead compounds to accelerate their translation towards therapeutic applications. To date, CRBN has been successfully utilized as the E3 ligase in PROTACs, targeting more than 100 different proteins, ranging from those involved in various cancers and immune disorders, to neurodegenerative disease-associated proteins, and even viral proteins. Furthermore, our developed indazolone-based architectures can serve as novel CRBN binders for the design of diverse PROTACs to address challenging diseases.

Conclusion

In summary, our work introduces an innovative indazolone-based platform that critically advances MGD discovery by moving beyond the canonical isoindolinone-glutarimide scaffolds, thereby expanding the chemical space. We leveraged mechanistic insights into CRBN-MGD complex conformational plasticity to rationally design indazolone architectures, establishing a robust foundation for next-generation MGDs. Crucially, this platform provides unprecedented programmability of CRBN substrate specificity, enabling the fine-tuned control of neo-substrate recognition—from multi-target to exquisitely selective degradation profiles (e.g., IKZF1/3, CK1α, IKZF2). This innovation not only expands the chemical space for CRBN-MGDs, converting previously undruggable proteins into tractable therapeutic targets, but also creates novel therapeutic strategies for challenging diseases like

hematological malignancies and solid tumors. Collectively, the indazolone architecture's remarkable tunability, demonstrated target degradation efficacy, and favorable pharmacokinetic properties establish it as a powerful blueprint for future CRBN-based MGD development. Furthermore, our developed indazolone architectures offer novel CRBN ligands for the rational design of diverse PROTACs, significantly broadening the scope of TPD therapeutics and paving the way for systematically addressing intractable diseases.

Supporting Information

Supporting Figures, ^{1}H and ^{13}C NMR spectra for all compounds, additional experimental details, materials and methods, and tables.

Notes

The authors declare no competing financial interest.

Acknowledgements

This study was supported by the National Science Foundation of China (No. 22377136 to X.-H. C); the Strategic Priority Research Program of the Chinese Academy of Science (XDB1260202 to X.-H. C.). the Science and Technology Commission of Shanghai Municipality, China (No.25ZR1402553 to H.-J. N).

Reference

[1] M. Békés, D. R. Langley, C. M. Crews, PROTAC targeted protein degraders: the past is prologue. *Nat. Rev. Drug Discov.* **2022**, *21*, 181-200.

[2] M. Hinterndorfer, V. A. Spiteri, A. Ciulli, G. E. Winter, Targeted protein degradation for cancer therapy. *Nat. Rev. Cancer* **2025**, 25, 493–516.

[3] J. M. Tsai, R. P. Nowak, B. L. Ebert, E. S. Fischer, Targeted protein degradation: from mechanisms to clinic. *Nat. Rev. Mol. Cell Biol.* **2024**, *25*, 740-757.

[4] B. Dale, M. Cheng, K.-S. Park, H. Ü. Kaniskan, Y. Xiong, J. Jin, Advancing targeted protein degradation for cancer therapy. *Nat. Rev. Cancer* **2021**, *21*, 638-654.

[5] K. M. Sakamoto, K. B. Kim, A. Kumagai, F. Mercurio, C. M. Crews, R. J. Deshaies, Protacs: Chimeric molecules that target proteins to the Skp1–Cullin–F box complex for ubiquitination and degradation. *Proc. Natl. Acad. Sci. U.S.A.* **2001**, *98*, 8554-8559.

[6] S. L. Schreiber, The rise of molecular glues. *Cell* **2021**, *184*, 3-9.

[7] Z. Kozicka, N. H. Thomä, Haven't got a glue: Protein surface variation for the design of molecular glue degraders. *Cell Chem. Biol.* **2021**, *28*, 1032-1047.

[8] E. R. Watson, S. Novick, M. E. Matyskiela, P. P. Chamberlain, A. H. de la Peña, J. Zhu, E. Tran, P. R. Griffin, I. E. Wertz, G. C. Lander, Molecular glue CELMoD compounds are regulators of cereblon conformation. *Science* **2022**, *378*, 549-553.

[9] Y. Liu, J. Bai, D. Li, Y. Cang, Routes to molecular glue degrader discovery. *Trends Biochem. Sci.* **2025**, *50*, 134-142.

[10] V. Oleinikovas, P. Gainza, T. Ryckmans, B. Fasching, N. H. Thomä, From thalidomide to rational molecular glue design for targeted protein degradation. *Annu. Rev. Pharmacol. Toxicol.* **2024**, *64*, 291-312.

[11] Q. L. Sievers, G. Petzold, R. D. Bunker, A. Renneville, M. Słabicki, B. J. Liddicoat, W. Abdulrahman, T. Mikkelsen, B. L. Ebert, N. H. Thomä, Defining the human C2H2 zinc finger degrome targeted by thalidomide analogs through CRBN. *Science* **2018**, *362*, eaat0572.

[12] G. Petzold, P. Gainza, S. Annunziato, I. Lamberto, P. Trenh, L. A. McAllister, B. DeMarco, L. Schwander, R. D. Bunker, M. Zlotosch, R. SriRamaratnam, S. Gilberto, G. Langousis, E. J. Donckele, C. Quan, V. Strande, G. M. De Donatis, S. B. Alabi, J. Alers, M. Matysik, C. Staehly, A. Dubois, A. Osmont, M. Garskovas, D. Lyon, L. Wiedmer, V. Oleinikovas, R. Lieberherr, N. T. Rubin, D. T. Lam, X. Lucas, E. Liardo, N. I. Widlund, A. Ritzén, R. M. Caceres, D. Vigil, J. Tsai, O. Wallace, M. Peluso, A. Sadok, R. Tiedt, A. M. Paterson, V. Zarayskiy, B. Fasching, D. Bonenfant, M. Warmuth, J. C. Castle, S. A. Townson, Mining the CRBN target space redefines rules for molecular glue–induced neosubstrate recognition. *Science* **2025**, *389*, eadt6736.

[13] M. Konstantinidou, M. R. Arkin, Molecular glues for protein-protein interactions: Progressing toward a new dream. *Cell Chem. Biol*. **2024**, *31*, 1064-1088.

[14] A. Domostegui, L. Nieto-Barrado, C. Perez-Lopez, C. Mayor-Ruiz, Chasing molecular glue degraders: screening approaches. *Chem. Soc. Rev*. **2022**, *51*, 5498-5517.

[15] G. Dong, Y. Ding, S. He, C. Sheng, Molecular glues for targeted protein degradation: from serendipity to rational discovery. *J. Med. Chem.* **2021**, *64*, 10606-10620.

[16] Y. Xu, W. Zhao, H.-J. Nie, J. Wang, J. Fu, H. Hu, Z. Liu, S. Tao, M. Zhang, Y. Zhou, J. Li, M. Tan, X.-H. Chen, Cross-Linking Profiling of Molecular Glue Degrader-Induced E3 Ligase Interactome to Expand Target Space. *Angew. Chem. Int. Ed.* **2025**, *64*, e202505053.

[17] K. Baek, R. J. Metivier, S. S. Roy Burman, J. W. Bushman, H. Yoon, R. J. Lumpkin, J. K. Ryan, D. M. Abeja, M. Lakshminarayan, H. Yue, S. Ojeda, Y. Xiong, J. Che, A. L. Verano, A. M. Schmoker, N. S. Gray, K. A. Donovan, E. S. Fischer, Unveiling the hidden interactome of CRBN molecular glues. *Nat. Commun.* **2025**, *16*, 6831.

[18] T. Ito, H. Ando, T. Suzuki, T. Ogura, K. Hotta, Y. Imamura, Y. Yamaguchi, H. Handa, Identification of a primary target of thalidomide teratogenicity, *Science* **2010**, *327*, 1345-1350.

[19] E. C. Fink, B. L. Ebert, The novel mechanism of lenalidomide activity, *Blood* **2015**, *126*, 2366-2369.

[20] J. Yamamoto, T. Ito, Y. Yamaguchi, H. Handa, Discovery of CRBN as a target of thalidomide: a breakthrough for progress in the development of protein degraders, *Chem. Soc. Rev.* **2022**, *51*, 6234-6250.

[21] J. Kronke, N. D. Udeshi, A. Narla, P. Grauman, S. N. Hurst, M. McConkey, T. Svinkina, D. Heckl, E. Comer, X. Li, C. Ciarlo, E. Hartman, N. Munshi, M. Schenone, S. L. Schreiber, S. A. Carr, B. L. Ebert, Lenalidomide causes selective degradation of IKZF1 and IKZF3 in multiple myeloma cells, *Science* **2014**, *343*, 301-305.

[22] M. E. Matyskiela, W. Zhang, H. W. Man, G. Muller, G. Khambatta, F. Baculi, M. Hickman, L. LeBrun, B. Pagarigan, G. Carmel, C. C. Lu, G. Lu, M. Riley, Y. Satoh, P. Schafer, T. O. Daniel, J. Carmichael, B. E. Cathers, P. P. Chamberlain, A Cereblon Modulator (CC-220) with Improved Degradation of Ikaros and Aiolos, *J. Med. Chem.* **2018**, *61*, 535-542.

[23] J. D. Hansen, M. Correa, M. A. Nagy, M. Alexander, V. Plantevin, V. Grant, B. Whitefield, D. Huang, T. Kercher, R. Harris, R. K. Narla, J. Leisten, Y. Tang, M. Moghaddam, K. Ebinger, J. Piccotti, C. G. Havens, B. Cathers, J. Carmichael, T. Daniel, R. Vessey, L. G. Hamann, K. Leftheris, D. Mendy, F. Baculi, L. A. LeBrun, G. Khambatta, A. Lopez-Girona, Discovery of CRBN E3 Ligase Modulator CC-92480 for the Treatment of Relapsed and Refractory Multiple Myeloma, *J. Med. Chem.* **2020**, *63*, 6648-6676.

[24] P. Li, X. Hu, Z. Fan, S. Sun, Q. Ran, T. Wei, P. Wei, Q. Jiang, J. Yan, N. Yang, C. Jia, T. Yang, Y. Mao, X. Cai, T. Xu, Z. Zhao, X. Qian, W. Qin, X. Zhuang, F. Fan, J. Xiao, Z. Zheng, S. Li, Novel potent molecular glue degraders against broad range of hematological cancer cell lines via multiple neosubstrates degradation, *J. Hematol. Oncol.* **2024**, *17*, 77.

[25] J. Kronke, E. C. Fink, P. W. Hollenbach, K. J. MacBeth, S. N. Hurst, N. D. Udeshi, P. P. Chamberlain, D. R. Mani, H. W. Man, A. K. Gandhi, T. Svinkina, R. K. Schneider, M. McConkey, M. Jaras, E. Griffiths, M. Wetzler, L. Bullinger, B. E. Cathers, S. A. Carr, R. Chopra, B. L. Ebert, Lenalidomide induces ubiquitination and degradation of CK1alpha in del(5q) MDS, *Nature* **2015**, *523*, 183-188.

[26]M. Teng, W. Lu, K. A. Donovan, J. Sun, N. M. Krupnick, R. P. Nowak, Y. D. Li, A. S. Sperling, T.

Zhang, B. L. Ebert, E. S. Fischer, N. S. Gray, Development of PDE6D and CK1alpha Degraders through Chemical Derivatization of FPFT-2216, *J. Med. Chem.* **2022**, *65*, 747-756.

[27] S. M. Park, D. K. Miyamoto, G. Y. Q. Han, M. Chan, N. M. Curnutt, N. L. Tran, A. Velleca, J. H. Kim, A. Schurer, K. Chang, W. Xu, M. G. Kharas, C. M. Woo, Dual IKZF2 and CK1alpha degrader targets acute myeloid leukemia cells, *Cancer Cell* **2023**, *41*, 726-739 e711.

[28] G. Nishiguchi, L. G. Mascibroda, S. M. Young, E. A. Caine, S. Abdelhamed, J. J. Kooijman, D. J. Miller, S. Das, K. McGowan, A. Mayasundari, Z. Shi, J. M. Barajas, R. Hiltenbrand, A. Aggarwal, Y. Chang, V. Mishra, S. Narina, M. Thomas, A. J. Loughran, R. Kalathur, K. Yu, S. Zhou, X. Wang, A. A. High, J. Peng, S. M. Pruett-Miller, D. L. Daniels, M. Urh, A. A. Shelat, C. G. Mullighan, K. M. Riching, G. J. R. Zaman, M. Fischer, J. M. Klco, Z. Rankovic, Selective CK1alpha degraders exert antiproliferative activity against a broad range of human cancer cell lines, *Nat. Commun.* **2024**, *15*, 482.

[29] Q. Geng, Z. Jiang, W. S. Byun, K. A. Donovan, Z. Zhuang, F. Jiang, H. M. Jones, H. Razumkov, M. T. Tang, R. C. Sarott, E. S. Fischer, S. M. Corsello, S. M. Hinshaw, N. S. Gray, Development of Potent and Selective CK1alpha Molecular Glue Degraders, *J. Med. Chem.* **2025**, *68*, 3180-3196.

[30] V. N. Dippon, Z. Rizvi, A. E. Choudhry, C. W. Chung, I. F. Alkuraya, W. Xu, X. B. Tao, A. J. Jurewicz, J. L. Schneck, W. Chen, N. M. Curnutt, F. Kabir, K. H. Chan, M. A. Queisser, C. Musetti, H. Dai, G. C. Lander, A. B. Benowitz, C. M. Woo, Identification of an allosteric site on the E3 ligase adapter cereblon, *Nature* **2026**.

[31] M. E. Matyskiela, G. Lu, T. Ito, B. Pagarigan, C. C. Lu, K. Miller, W. Fang, N. Y. Wang, D. Nguyen, J. Houston, G. Carmel, T. Tran, M. Riley, L. Nosaka, G. C. Lander, S. Gaidarova, S. Xu, A. L. Ruchelman, H. Handa, J. Carmichael, T. O. Daniel, B. E. Cathers, A. Lopez-Girona, P. P. Chamberlain, A novel cereblon modulator recruits GSPT1 to the CRL4(CRBN) ubiquitin ligase, *Nature* **2016**, *535*, 252-257.

[32] C. Surka, L. Jin, N. Mbong, C. C. Lu, I. S. Jang, E. Rychak, D. Mendy, T. Clayton, E. Tindall, C. Hsu, C. Fontanillo, E. Tran, A. Contreras, S. W. K. Ng, M. Matyskiela, K. Wang, P. Chamberlain, B. Cathers, J. Carmichael, J. Hansen, J. C. Y. Wang, M. D. Minden, J. Fan, D. W. Pierce, M. Pourdehnad, M. Rolfe, A. Lopez-Girona, J. E. Dick, G. Lu, CC-90009, a novel cereblon E3 ligase modulator, targets acute myeloid leukemia blasts and leukemia stem cells, *Blood* **2021**, *137*, 661-677.

[33] Y. Chang, F. Keramatnia, P. S. Ghate, G. Nishiguchi, Q. Gao, I. Iacobucci, L. Yang, D. Chepyala, A. Mishra, A. A. High, H. Goto, K. Akahane, J. Peng, J. J. Yang, M. Fischer, Z. Rankovic, C. G. Mullighan, The orally bioavailable GSPT1/2 degrader SJ6986 exhibits in vivo efficacy in acute lymphoblastic leukemia, *Blood* **2023**, *142*, 629-642.

[34] Y. Liu, X. Sun, Q. Liu, C. Han, Y. Rao, A Dual-Target and Dual-Mechanism Design Strategy by Combining Inhibition and Degradation Together, *J. Am. Chem. Soc.* **2025**, *147*, 3110-3118.

[35] E. S. Wang, A. L. Verano, R. P. Nowak, J. C. Yuan, K. A. Donovan, N. A. Eleuteri, H. Yue, K.

H. Ngo, P. H. Lizotte, P. C. Gokhale, N. S. Gray, E. S. Fischer, Acute pharmacological degradation of Helios destabilizes regulatory T cells, *Nat. Chem. Biol.* **2021**, *17*, 711-717.

[36] S. Bonazzi, E. d'Hennezel, R. E. J. Beckwith, L. Xu, A. Fazal, A. Magracheva, R. Ramesh, A. Cernijenko, B. Antonakos, H. C. Bhang, R. G. Caro, J. S. Cobb, E. Ornelas, X. Ma, C. A. Wartchow, M. C. Clifton, R. R. Forseth, B. H. Fortnam, H. Lu, A. Csibi, J. Tullai, S. Carbonneau, N. M. Thomsen, J. Larrow, B. Chie-Leon, D. Hainzl, Y. Gu, D. Lu, M. J. Meyer, D. Alexander, J. Kinyamu-Akunda, C. A. Sabatos-Peyton, N. A. Dales, F. J. Zecri, R. K. Jain, J. Shulok, Y. K. Wang, K. Briner, J. A. Porter, J. A. Tallarico, J. A. Engelman, G. Dranoff, J. E. Bradner, M. Visser, J. M. Solomon, Discovery and characterization of a selective IKZF2 glue degrader for cancer immunotherapy, *Cell Chem Biol* **2023**, *30*, 235-247 e212.

[37] D. K. Miyamoto, N. M. Curnutt, S. M. Park, A. Stavropoulos, M. G. Kharas, C. M. Woo, Design and Development of IKZF2 and CK1alpha Dual Degraders, *J. Med. Chem.* **2023**, *66*, 16953-16979.

[38]Z. Chen, H. Dhruv, X. Zhang, R. K. Rej, L. Bai, D. McEachern, P. Kirchhoff, R. Nagilla, L. J. Jolivette, C. T. Rice, P. Orth, C. O. Strickland, E. S. Priestley, H. P. Mohammad, M. Wang, B. Wen, D. Sun, Z. Sui, S. Wang, Development of PVTX-405 as a potent and highly selective molecular glue degrader of IKZF2 for cancer immunotherapy, *Nat. Commun.* **2025**, *16*, 4095.

[39] P. Y. Ting, S. Borikar, J. R. Kerrigan, N. M. Thomsen, E. Aghania, A. E. Hinman, A. Reyes, N. Pizzato, B. D. Fodor, F. Wu, M. S. Belew, X. Mao, J. Wang, S. Chitnis, W. Niu, A. Hachey, J. S. Cobb, N. A. Savage, A. Burke, J. Paulk, D. Dovala, J. Lin, M. C. Clifton, E. Ornelas, X. Ma, N. F. Ware, C. C. Sanchez, J. Taraszka, R. Terranova, J. Knehr, M. Altorfer, S. W. Barnes, R. E. J. Beckwith, J. M. Solomon, N. A. Dales, A. W. Patterson, J. Wagner, T. Bouwmeester, G. Dranoff, S. C. Stevenson, J. E. Bradner, A molecular glue degrader of the WIZ transcription factor for fetal hemoglobin induction, *Science* **2024**, *385*, 91-99.

[40] J. R. Kerrigan, N. M. Thomsen, A. Cernijenko, S. E. Kochanek, J. Dewhurst, G. O'Brien, N. F. Ware, C. C. Sanchez, J. R. Manning, X. Ma, E. Ornelas, N. A. Savage, J. R. Partridge, A. W. Patterson, P. Lam, N. A. Dales, S. Bonazzi, S. Borikar, A. E. Hinman, P. Y. Ting, Discovery and Optimization of First-in-Class Molecular Glue Degraders of the WIZ Transcription Factor for Fetal Hemoglobin Induction to Treat Sickle Cell Disease, *J. Med. Chem.* **2024**, *67*, 20682-20694.

[41] H. Razumkov, Z. Jiang, K. Baek, I. You, Q. Geng, K. A. Donovan, M. T. Tang, R. J. Metivier, N. Mageed, P. Seo, Z. Li, W. S. Byun, S. M. Hinshaw, R. C. Sarott, E. S. Fischer, N. S. Gray, Discovery of CRBN-Dependent WEE1 Molecular Glue Degraders from a Multicomponent Combinatorial Library, *J. Am. Chem. Soc.* **2024**, *146*, 31433-31443.

[42] H. Lin, X. Yu, Haiyang, R. Cheng, X. Qi, Y. Y. Yang, S. Zhou, X. Che, J. Wang, Beyond the G-Loop: CRBN Molecular Glues Potently Target VAV1 via a Novel SH3 RT-Loop Degron, *bioRxiv* **2025**. doi: https://doi.org/10.1101/2025.06.08.658535

[43] L. Chen, L. Huang, W. Wen, P. Zeng, Y. Wu, Q. Han, X. Chen, Z. Guo, H. Yu, W. Lu, B. Jiang, Selective and Potent Molecular Glue Degraders for NIMA-Related Kinase 7, *Angew. Chem. Int. Ed.* **2025**, *64*, e202500169.

[44] A. Sylvain, N. Stoehr, F. Ma, A. Cernijenko, M. Schroder, M. Khoshouei, M. Vogelsanger, M. Schoenboerner, A. Burke, P. Rao, J. M. Solomon, J. Paulk, L. Xu, J. Dawson, D. Begue, P. Lefeuvre, E. Ahrne, A. Hofmann, C. J. Dickson, P. Arabin, A. Zimmerlin, M. Kiffe, M. Froehlicher, T. Boersig, A. Elhajouji, M. Brichet, S. Menon, S. Liu, M. Mueller, C. A. Wartchow, J. Lin, Y. C. Gloria, S. Dickhofer, A. N. R. Weber, T. Welzel, J. Kuemmerle-Deschner, C. J. Farady, R. Pulz, F. Bornancin, D. L. Buckley, Z. I. Bassi, A cereblon-based glue degrader of NEK7 regulates NLRP3 inflammasome in a context-dependent manner, *Cell Chem Biol* **2025**, *32*, 955-968 e913.

[45] M. Steger, G. Nishiguchi, Q. Wu, B. Schwalb, B. Shashikadze, K. McGowan, M. Actis, A. Aggarwal, Z. Shi, J. Price, A. Mayasundari, L. Yang, A. H. Bednarz, S. Machata, T. Graef, D. Bartoschek, V. Demichev, U. Ohmayer, J. Yang, H. Daub, Z. Rankovic, Unbiased mapping of cereblon neosubstrate landscape by high-throughput proteomics, *Nat. Commun.* **2025**, *16*, 7773.

[46] J. An, X. Zhang, Crbn-based molecular Glues: Breakthroughs and perspectives, *Bioorg. Med. Chem.* **2024**, *104*, 117683.

[47] M. J. Nutt, S. G. Stewart, Strengthening Molecular Glues: Design Strategies for Improving Thalidomide Analogs as Cereblon Effectors and Anticancer Agents, *Drug Discov. Today* **2024**, *29*, 104010.

[48] J. M. Sasso, R. Tenchov, D. Wang, L. S. Johnson, X. Wang, Q. A. Zhou, Molecular Glues: The Adhesive Connecting Targeted Protein Degradation to the Clinic, *Biochemistry* **2023**, *62*, 601-623.

[49] J. Min, A. Mayasundari, F. Keramatnia, B. Jonchere, S. W. Yang, J. Jarusiewicz, M. Actis, S. Das, B. Young, J. Slavish, L. Yang, Y. Li, X. Fu, S. H. Garrett, M. K. Yun, Z. Li, S. Nithianantham, S. Chai, T. Chen, A. Shelat, R. E. Lee, G. Nishiguchi, S. W. White, M. F. Roussel, P. R. Potts, M. Fischer, Z. Rankovic, Phenyl-Glutarimides: Alternative Cereblon Binders for the Design of PROTACs, *Angew. Chem. Int. Ed.* **2021**, *60*, 26663-26670.

[50] C. Steinebach, A. Bricelj, A. Murgai, I. Sosic, L. Bischof, Y. L. D. Ng, C. Heim, S. Maiwald, M. Proj, R. Voget, F. Feller, J. Kosmrlj, V. Sapozhnikova, A. Schmidt, M. R. Zuleeg, P. Lemnitzer, P. Mertins, F. K. Hansen, M. Gutschow, J. Kronke, M. D. Hartmann, Leveraging Ligand Affinity and Properties: Discovery of Novel Benzamide-Type Cereblon Binders for the Design of PROTACs, *J. Med. Chem.* **2023**, *66*, 14513-14543.

[51] S. Norris, X. Ba, J. Rhodes, D. Huang, G. Khambatta, J. Buenviaje, S. Nayak, J. Meiring, S. Reiss, S. Xu, L. Shi, B. Whitefield, M. Alexander, E. J. Horn, M. Correa, L. Tehrani, J. D. Hansen, P. Papa, D. S. Mortensen, Design and Synthesis of Novel Cereblon Binders for Use in Targeted Protein Degradation, *J. Med. Chem.* **2023**, *66*, 16388-16409.

[52] Y. Zhou, S. L. Garrigues, E. Villemure, N. Ishisoko, H. Q. Nguyen, N. K. Hamidi, R. Vogt, Y. Wang, R. A. Blake, J. Rudolph, C. Nilewski, Heteroaryl Glutarimides and Dihydrouracils as Cereblon Ligand Scaffolds for Molecular Glue Degrader Discovery, *ACS Med. Chem. Lett.* **2024**, *15*, 2158-2163.

[53] X. Nie, Y. Zhao, H. Tang, Z. Zhang, J. Liao, C. M. Almodovar-Rivera, R. Sundaresan, H. Xie, L. Guo, B. Wang, H. Guan, Y. Xing, W. Tang, Development of Phenyl-substituted Isoindolinone- and Benzimidazole-type Cereblon Ligands for Targeted Protein Degradation, *ChemBioChem* **2024**, *25*, e202300685.

[54] A. Kazantsev, M. Krasavin, Ligands for cereblon: 2017-2021 patent overview, *Expert Opin. Ther. Pat.* **2022**, *32*, 171-190.

[55] X. Han, Y. Sun, PROTACs: A novel strategy for cancer drug discovery and development, *MedComm* **2023**, *4*, e290.

[56] J. L. Gray, Z. Xiao, V. V. Rogga, X. Zhang, E. W. Tate, From Serendipity to Strategy: Rationalizing Molecular Glue Discovery and Proximity-Induced Pharmacology through Chemical Biology, *J. Am. Chem. Soc.* **2026**, *148*, 4791-4814.

[57] G. Petzold, E. S. Fischer, N. H. Thoma, Structural basis of lenalidomide-induced CK1alpha degradation by the CRL4(CRBN) ubiquitin ligase, *Nature* **2016**, *532*, 127-130.

[58] H. Hu, H. J. Nie, X. H. Chen, Primary Amine-Based Photoclick Chemistry: From Concept to Diverse Applications in Chemical Biology and Medicinal Chemistry. *Acc. Chem. Res.* **2025**, *58*, 1963-1981.

[59] A.-D. Guo, D. Wei, H.-J. Nie, H. Hu, C. Peng, S.-T. Li, K.-N. Yan, B.-S. Zhou, L. Feng, C. Fang, M. Tan, R. Huang, X.-H. Chen, Light-induced primary amines and o-nitrobenzyl alcohols cyclization as a versatile photoclick reaction for modular conjugation. *Nat. Commun.* **2020**, *11*, 5472.

[60] K. N. Yan, Y. Q. Nie, J. Y. Wang, G. L. Yin, Q. Liu, H. Hu, X. Sun, X. H. Chen, Accelerating PROTACs Discovery Through a Direct-to-Biology Platform Enabled by Modular Photoclick Chemistry. *Adv. Sci.* **2024**, *11*, 2400594.

[61] A.-D. Guo, K.-N. Yan, H. Hu, L. Zhai, T.-F. Hu, H. Su, Y. Chi, J. Zha, Y. Xu, D. Zhao, X. Lu, Y.-J. Xu, J. Zhang, M. Tan, X.-H. Chen, Spatiotemporal and global profiling of DNA–protein interactions enables discovery of low-affinity transcription factors. *Nat. Chem.* **2023**, *15*, 803-814.

[62] H. Hu, W. Hu, A.-D. Guo, L. Zhai, S. Ma, H.-J. Nie, B.-S. Zhou, T. Liu, X. Jia, X. Liu, X. Yao, M. Tan, X.-H. Chen, Spatiotemporal and direct capturing global substrates of lysine-modifying enzymes in living cells. Nat. Commun. 2024, 15, 1465.

[63] H.-J. Nie, H. Hu, X. Qi, Y.-J. Zhou, L. Liu, X.-H. Chen, General Platform for Efficient and Modular Assembly of GalNAc–siRNA Conjugates via Primary Amines and o-Nitrobenzyl Alcohol Cyclization Photoclick Chemistry Enabling Rapid Access to Therapeutic Oligonucleotides. JACS Au 2025, 5, 1402-1412.

[64] Y. Xu, H. Hu, Y. Ran, W. Zhao, A. D. Guo, H. J. Nie, L. Zhai, G. L. Yin, J. Cheng, S. Tao, B. Yang, M. Tan, X. H. Chen, Visible-Light-Controlled Lysine-Selective Crosslinking Decodes Protein Complexes and Dynamic Interactomes in Live Cells. *Angew. Chem. Int. Ed.* **2025**, *64*, e202507254.

[65] T. V. Sharp, F. Munoz, D. Bourboulia, N. Presneau, E. Darai, H. W. Wang, M. Cannon, D. N. Butcher, A. G. Nicholson, G. Klein, S. Imreh, C. Boshoff, LIM domains-containing protein 1 (LIMD1), a tumor suppressor encoded at chromosome 3p21.3, binds pRB and represses E2F-driven transcription, *Proc. Natl. Acad. Sci. U. S. A.* **2004**, *101*, 16531-16536.

[66] T. V. Sharp, A. Al-Attar, D. E. Foxler, L. Ding, A. V. T. Q. de, Y. Zhang, H. S. Nijmeh, T. M. Webb, A. G. Nicholson, Q. Zhang, A. Kraja, I. Spendlove, J. Osborne, E. Mardis, G. D. Longmore, The chromosome 3p21.3-encoded gene, LIMD1, is a critical tumor suppressor involved in human lung cancer development, *Proc. Natl. Acad. Sci. U. S. A.* **2008**, *105*, 19932-19937.

[67] D. E. Foxler, K. S. Bridge, V. James, T. M. Webb, M. Mee, S. C. Wong, Y. Feng, D. Constantin-Teodosiu, T. E. Petursdottir, J. Bjornsson, S. Ingvarsson, P. J. Ratcliffe, G. D. Longmore, T. V. Sharp, The LIMD1 protein bridges an association between the prolyl hydroxylases and VHL to repress HIF-1 activity, *Nat. Cell Biol.* **2012**, *14*, 201-208.

[68] I. Baine, S. Basu, R. Ames, R. S. Sellers, F. Macian, Helios induces epigenetic silencing of IL2 gene expression in regulatory T cells, *J. Immunol.* **2013**, *190*, 1008-1016.